X-100, 100 μg/ml bovine serum albumin, 200 mM NaCl, and protease inhibitor mixture. After 2 h under rotation at 4 °C, the samples were washed five times with PBS supplemented with 0.2% Triton X-100. Bound SR was analyzed by SDS-Page and Western blot analysis with a rabbit anti-SR serum (1:1000) characterized previously (8).

Preparation of FBXO22 Deletion Mutants—To delete the F-box region (ΔFBXO22 construct), we carried out PCR with PfuUltra high fidelity (HF) polymerase (Agilent) using primer pairs flanking the F-box region (between amino acids 20 and 68). The primers were as follows: primer 1, 5′ CGCGGCTCCTCCGTAGACCCGCGGAGCACCTGGATCTCCGCAGGC 3′, corresponding to amino acids 11–20 fused with amino acids 68–74; primer 2, 5′ ATAAGAATGCGGCCGCTTATTTAGATGACCCCAG 3′, complementary to the C-terminal region of FBXO22b with a restriction site for the NotI enzyme. After gel purification, the SalI site and amino acids 1–10 were inserted by PCR with primer 3 (5′ ACGCGTCGACCATGGAGCCGGTAGGCTGCGGCGAGTGCCGCGGCTCCTCCGTA 3′) and primer 2. The sequence was verified by double-stranded DNA sequence, and the desired product was inserted into the appropriate pRK5 plasmids.

Cell Culture and Transfection—HEK293, SH-SY5Y, or A172 cells were cultured in DMEM containing 10% FBS, antibiotics (penicillin, 100 units/ml; streptomycin, 0.1 mg/ml; and amphotericin B, 0.25 μg/ml) and 4 mM glutamine. Cells were plated on 6-well tissue culture plates (Nunc) and transfected after 24 h at 70–90% confluence using Lipofectamine 2000 (Invitrogen) with the indicated DNAs. Transfection of A172 cells was carried out without FBS or antibiotics. Cells were harvested 48–72 h post-transfection. Transfection of siRNA was carried out with 100 nM siRNA using Lipofectamine 2000 according to the specifications of the manufacturer, and cells were harvested 72 h after transfection. FBXO22 siRNA (Sigma), referred to as siRNA-988, consisted of 5′ GCCAUAAGAGAGCAAGGAA 3′.

Coimmunoprecipitations and Western Blot Analysis—HEK293A cells were cotransfected with Myc-FBXO22a and either HA-SR or HA-glucosamine 6-phosphate deaminase (GNPDA). Thirty-six hours after transfection, cells were lysed by gentle sonication in 20 mM Tris-HCl (pH 7.4), 1 mM EDTA, 30 μM MG132, 300 mM NaCl, and protease inhibitor mixture. After sonication, Triton X-100 was added to 1% final concentration, and the suspension was cleared by centrifugation at 16,000 × *g* for 10 min. Myc-FBXO22a was immunoprecipitated by adding anti-Myc matrix (Sigma) for 2 h under rotation at 4 °C. After washing six times with high stringency buffer consisting of 20 mM Tris-HCl (pH 7.4), 300 mM NaCl, and 1% Triton X-100, the immunoprecipitates were analyzed by SDS-PAGE and Western blot using mouse anti-HA 1:1000 (Sigma) and rabbit anti-Myc 1:500 (Sigma). Coimmunoprecipitation of SR and FBXO22b was carried out essentially as described above, except we employed overnight incubation with anti-HA matrix and 400 mM NaCl instead of 300 mM in the washing steps to prevent nonspecific binding.

To investigate the interaction of FBXO22 with the SCF complex, HEK293 cells were transfected with Myc-FBXO22b, Myc-FBXO22b Δ20–67, or Myc-FBXO22a. Thirty-six hours after transfection, MG132 (30 μM) was added for 12 h, and cells were lysed by gentle sonication in buffer containing 50 mM Tris-HCl (pH 7.4), 1 mM EDTA, 10% glycerol, 30 μM MG132, 140 mM NaCl, and protease inhibitor mixture. Then Nonidet P-40 was added to 1% final concentration, and the suspension was cleared by centrifugation for 10 min at 16,000 × *g* at 4 °C. Immunoprecipitation was performed with anti-Myc matrix (Sigma) for 3 h at 4 °C. The beads were washed six times with 50 mM Tris-HCl (pH 7.4), 10% glycerol, 140 mM NaCl, and 1% Nonidet P-40. The Western blot was probed using mouse anti-Cul1 1:500 (BD Biosciences), mouse anti-Skp1 1:500 (BD Biosciences), and mouse anti-Myc 1:2500 (Sigma).

For the endogenous interaction of SR with FBXO22, rat brains were homogenized using a glass homogenizer with 5 volumes of 50 mM Tris-HCl (pH 7.4), 140 mM NaCl, 1% CHAPS, 30 μM MG132, and protease inhibitor mixture. The homogenate was cleared by centrifugation at 30,000 × *g* for 20 min at 4 °C. 10 μg of purified anti-SR and rabbit normal IgG was coupled to protein G-agarose using dimethylpimelimidate (Sigma) as described previously (32) and incubated for 12 h with rat brain homogenate at 1.5 mg/ml. The immunoprecipitate was washed six times with 50 mM Tris-HCl (pH 7.4), 140 mM NaCl, and 0.5% CHAPS, and the coimmunoprecipitation was revealed with mouse anti-FBXO22 (1:100, Santa Cruz Biotechnology) and rabbit anti-SR serum (1:1000).

To investigate whether SR associates with $SCF^{hFBXO22a}$, we employed conditions as described previously (33), with slight modifications. HEK293 cells were cotransfected with HA-hFBXO22a and Myc-KDM4A or Myc-SR. Forty-eight hours post-transfection, cells were lysed for 30 min on ice in buffer containing 50 mM Tris-HCl (pH 7.4), 150 mM NaCl, 1 mM EDTA, 0.2% Nonidet P-40, and protease inhibitor mixture (Mini Complete, Roche Diagnostics). The lysate was cleared by centrifugation at 14,000 × *g* for 10 min, and the immunoprecipitation was carried out using anti-Myc matrix (Sigma). After washing six times with lysis buffer, the samples were analyzed by SDS-PAGE and Western blot. In some experiments, HA-SR of HA-FBXO22a was cotransfected with either mouse Cul1 or mouse Skp1a in the pCMV-Sport6 vector (GE Healthcare), and coimmunoprecipitations were carried out as described above. To quantify the Western blots, the densitometry of the bands were calculated at the linear phase and divided by β-tubulin in each lane.

In Vivo Ubiquitination—HEK293 cells were transfected with FLAG-ubiquitin, HA-SR, and either GFP or Myc-hFBXO22a in the pRK5 plasmid. Twenty-four hours after transfection, cells were incubated with 30 μM MG132 for 12 h. Immunoprecipitation was carried out as described previously (34), with some modifications. Briefly, the cells were lysed by sonication in medium containing 10 mM Tris-HCl (pH 7.4), 1 mM EDTA, 20 mM *N*-ethylmaleimide, and protease inhibitor mixture. Subsequently, SDS was added to 1% final concentration, and the samples were boiled for 5 min. This was followed by a 10-fold dilution in buffer containing 20 mM Tris-HCl (pH 7.4), 2% Triton X-100, 0.5% deoxycholate, 1 mM EDTA, 100 mM NaCl, and protease inhibitor mixture. After centrifugation at 16,000 × *g* for 10 min to remove any insoluble material, the immunoprecipitation was carried out with anti-HA affinity matrix, and the immunoprecipitates were washed six times with 20 mM Tris-

HCl (pH 7.4), 200 mM NaCl, 0.5% deoxycholate, 0.1% SDS, and 1% Triton X-100. Subsequently, FLAG-ubiquitin-SR conjugates were revealed with rabbit anti-FLAG (1:1000), and total immunoprecipitated SR was monitored with mouse anti-HA (1:1000).

Pulse-Chase Experiments—Half-life experiments were carried out as described previously (35), with the following modifications. HEK293 cells were transfected with HA-SR and hFBXO22a, hFBXO22b, or GFP at a SR/hFBXO22 cDNA ratio of 1:14. Forty-eight hours after transfection, the medium was replaced by DMEM lacking methionine/cysteine (Sigma) for 1 h. Then the cells were pulsed with methionine/cysteine-free medium containing 100 μCi of [^{35}S]methionine/cysteine (PerkinElmer Life Sciences) for 70 min and subsequently chased in complete DMEM. At the specified times, the cells were harvested and lysed in buffer containing 20 mM Tris-HCl (pH 7.4), 0.3 M NaCl, 1% Triton X-100, 30 μM MG132, and protease inhibitors (Mini-complete, Roche Diagnostics). Immunoprecipitation of HA-SR was carried out with anti-HA affinity matrix (Covance), and the immunoprecipitates were washed six times with radioimmune precipitation assay buffer. The samples were resolved on SDS-PAGE gels, transferred to nitrocellulose membranes, and quantified by PhosphorImager analysis. The amount of immunoprecipitated HA-SR was checked by Western blot analysis, followed by densitometry of the chemiluminescent signal.

Brain Subcellular Fractionation—Brains of SR-KO mice (23) and WT controls were homogenized using a glass homogenizer with 5 volumes of 50 mM Tris-HCl (pH 7.4), 140 mM NaCl, 0.2% Triton X-100, 0.32 M sucrose, 1 mM $MgCl_2$, 1 mM potassium P_i, and Mini Complete (Roche Diagnostics). The homogenate was centrifuged at 1250 × *g* for 10 min at 4 °C to yield crude nuclear fraction (P1) and supernatant 1 (S1). After two washes by centrifugation in homogenization buffer, P1 was suspended in 2 M sucrose, layered over a 2.4 M sucrose cushion, and centrifuged at 53,000 × *g* for 75 min at 4 °C to yield a purified nuclear pellet (36). For obtaining the cytosolic fraction, the S1 fraction was centrifuged at 200,000 × *g* for 30 min to remove membranes.

For subcellular fractionation of A172 cultures, the cells were lysed by three freeze and thaw cycles in buffer containing 20 mM Tris-HCl (pH 7.4), 100 mM NaCl, and protease inhibitor mixture. An aliquot of the homogenate was put aside, and the remaining lysate was centrifuged at 1500 × *g* for 10 min (4 °C) to give a supernatant and crude nuclear pellet. P1 was washed twice by centrifugation and purified further to produce a purified nuclear fraction as described previously (36, 37), with the following modifications. P1 was suspended in 10 mM Tris-HCl (pH 7.4), 0.25% Triton X-100, 1 mM potassium P_i (pH 6.5), 1 mM $MgCl_2$, and 1.32 M sucrose supplemented with protease inhibitors and homogenized by six to seven strokes with a glass homogenizer. Subsequently, P1 was layered over a 1.7 M sucrose cushion and centrifuged at 53,000 × *g* for 75 min at 4 °C to obtain purified nuclei. Cytosolic and membrane fractions were obtained by centrifugation of S1 at 200,000 × *g* for 30 min. The membrane fraction was washed twice by centrifugation with lysis buffer.

Primary Cultures—Pregnant Sprague-Dawley rats were killed by quick decapitation following isoflurane anesthesia with the approval of the Committee for Supervision of Animal experiments (Technion-Israel Institute of Technology). Serum-free neuronal cultures from the cerebral cortex were prepared from E16–18 as described previously (24, 38) with the following modifications. The culture medium consisted of Neurobasal supplemented with B-27, 0.4 mM glutamine, and penicillin/streptomycin (Neurobasal + B-27). On DIV1, the cultured medium was changed to fresh Neurobasal + B27. Afterward, half of the culture media was replaced every 3 days to fresh Neurobasal + B27. Biochemical experiments were carried out on DIV10–12.

Primary astrocytic cultures were carried out with P0-P1 Sprague-Dawley rat pups as described previously (24). The cells were maintained in basal medium Eagle supplemented with 10% FBS, 0.4 mM glutamine, and penicillin/streptomycin and used at DIV14.

Lentivirus Production and shRNA-mediated Knockdown—A lentivirus harboring shRNA was produced by cotransfection of the pGIPZ vector (13 μg), pCMV-dR8.74 packing (8.7 μg), and VSVG envelope pMD2G (4.6 μg) in HEK293T cells (39). Medium containing virus was collected after 24 and 48 h post-transfection. The virus was concentrated by centrifugation at 116,000 × *g* for 2 h at 4 °C and resuspended in Neurobasal medium. Aliquots were stored at −70 °C until use. Primary neuronal cultures were infected on DIV4 with a multiplicity of infection of 30–50. Levels of FBXO22 were monitored by Western blot analysis with mouse anti-FBXO22 antibody (Sigma). Only cultures exhibiting at least 30–40% infection efficiency on DIV12–13 monitored by GFP fluorescence were employed. The pGIPZ construct containing FBXO22 shRNA (GE Healthcare) encompassed a mature antisense consisting of TATTCCTTCAATTTGAGGG (catalog no. RHS4430–98894301, referred to as 9889). Controls were carried out with pGIPZ non-silencing shRNA (catalog no. RHS4346, GE Healthcare).

Astrocytes were transduced at DIV10 with lentivirus harboring FBXO22-silencing or non-silencing shRNA (multiplicity of infection 20). The astrocytes were selected for 7 days with 2 μg/ml puromycin before use.

Immunocytochemistry—A172 cells were seeded on glass coverslips coated with poly-D-lysine (0.2–0.5 mg/ml) in 12-well plates at a concentration of 0.75–0.9 × 10^6 cells/well. After 72 h, cells were fixed for 20 min with fresh 4% paraformaldehyde. After washing with PBS, the cells were blocked and permeabilized at room temperature for 90 min with PBS supplemented with 8% normal goat serum, 80 mM NaCl, 2 mg/ml IgG-free BSA, and 0.1% Triton X-100. Colocalization was revealed by the use of serum anti-SR at 1:400 (8) and antibodies against FBXO22 (1:100) and KDEL (1:100) (Santa Cruz Biotechnology). Following primary antibody incubation for 16–20 h at 4 °C, the cells were blocked at room temperature with 6% normal goat serum (NGS) and 0.1% Triton X-100 in PBS. After washing the slides, anti-rabbit Cy3 and anti-mouse Cy2 were added to 4% NGS and 0.1% Triton X-100 in PBS. Afterward, the cells were washed, and DAPI was added for 30 s at a final concentration of 0.1 μg/ml for nuclear labeling, followed by three additional washes. Images were obtained using laser-scanning confocal microscopy (LSM 510 Meta laser-scanning confocal system (Zeiss)) with a ×63 oil objective. Optical sections of 2–3

μm were used at 1024 × 1024 pixel resolution. Final picture editing was done with 510 LSM software.

D-Serine Synthesis—For endogenous D-serine production, A172 cells were plated in 24-well plates at 0.1 × 10^6 cells/well and transfected with siRNA to FBXO22 or control siRNA as described in the previous section. Seventy-two hours after transfection, the cells were washed with basal medium Eagle containing 10% FCS and 4 mM glutamine. Then the medium was supplemented with 10 mM L-serine that was rendered free of contaminant D-serine as described previously (40). Synthesis of D-serine was monitored by HPLC of the culture media collected after 72 h and normalized by the SR expression levels in each well monitored by Western blot analysis and quantification using the Odissey system (LI-COR Biosciences). The identity of D-serine was confirmed by treating the media with recombinant D-serine deaminase from *E. coli* prior to HPLC analysis (40). In some experiments, D-serine was quantified by an enzymatic assay using recombinant yeast D-serine deaminase and Amplex Red (Invitrogen) amplification as described previously (41).

Serine Racemase Activity in Vitro—Recombinant His-SR (0.1 μg) was preincubated in PBS containing 3% glycerol and 5 μg of soluble GST-FBXO22a, GST-α-synuclein, or GST-CHIP (a 30- to 40 fold-excess of GST fusion proteins to SR monomer) for 1 h at 4 °C in silanized 1.5-ml polypropylene tubes. Subsequently, the samples were diluted 20-fold into reaction medium containing 20 mM Tris-HCl (pH 7.4), 1 mM $MgCl_2$, 100 μM ATP, 30 μM pyridoxal-5′-phosphate, 0.3 mM NADH, and 0.5 units/ml lactate dehydrogenase. SR activity was started by addition of 10 mM L-serine O-sulfate, an efficient SR substrate generating pyruvate, sulfate, and NH_4. Pyruvate was quantified by monitoring NADH absorbance as described previously (42).

RESULTS

To identify new SR interactors that regulate D-serine synthesis in cells, we carried out immunoprecipitation of HA-SR from SH-SY5Y neuroblastoma cells, followed by LC-MS analysis. The immunoprecipitate was washed extensively under high stringency conditions that favored the detection of strong interactors. Under these conditions, human FBXO22 (hFBXO22) was the only additional protein identified in the 36–42 kDa range of HA-SR gel bands, indicating the possible presence of a SR-FBXO22 complex (Fig. 1*A*).

Human FBXO22 protein contains an N-terminal F-box domain that mediates its interaction with the Skp1 component of the Skp1·Cullin·F-box (SCF) ubiquitin-ligase complex (43, 44). Analysis of the expressed sequence tag database indicates the existence of two FBXO22 isoforms, 22a and 22b (Fig. 1*A*). FBXO22a controls the degradation of KDM4A, a histone demethylase (33), and seems to be involved in the inflammatory response during *Salmonella* infection (45). In its C-terminal region, FBXO22a has an F-box intracellular transduction C-terminal domain (FIST C), presumably involved in amino acid sensing and signal transduction (46). The shorter and previously uncharacterized FBXO22b isoform lacks the FIST C region and differs in its 11 C-terminal amino acids because of alternative splicing (Fig. 1*A*). A search in the expressed sequence tags database revealed only two expressed sequence tags containing the shorter FBXO22b isoform compared with more than 100 expressed sequence tags containing FBXO22a, indicating that the latter is the dominant isoform.

To verify whether SR interacts directly with hFBXO22, we monitored the *in vitro* binding of purified His-tagged SR protein with purified GST-hFBXO22a and hFBXO22b fusion proteins in the presence of excess bovine serum albumin to prevent nonspecific binding (Fig. 1*B*). His-SR binds to hFBXO22 isoforms but not to GST-α-synuclein control protein, even when present at large excess, indicating that hFBXO22 directly interacts with SR (Fig. 1*B*).

To confirm that SR and hFBXO22 interact, we carried out coimmunoprecipitation from transfected HEK-293 cells. Myc-hFBXO22a coimmunoprecipitated with HA-SR (Fig. 1*C*) but not with unrelated control protein HA-GNPDA (Fig. 1*C*). A construct that mimics the smaller FBXO22 isoform, Myc-hFBXO22b (Fig. 1*D*), also coimmunoprecipitated with HA-SR but not with HA-FKBP12 (Fig. 1*D*). Immunoprecipitation of SR with the smaller isoform (hFBXO22b) that lacks the FIST C domain indicates that this region is not required for the interaction (Fig. 1*D*).

In contrast to hFBXO22a, the smaller hFBXO22b isoform displays only minimal binding to the Skp1 and Cul1 components of the SCF complex (Fig. 1*E*, compare *lanes 1* and *3*). Deletion of the F-Box domain (*Myc-hFBXO22b Δ20–67 mutant*) abrogates the association of hFBXO22 with the SCF complex, inferred from the lack of coimmunoprecipitation with Skp1 and Cul1 (Fig. 1*E*, *lane 2*). However, the Myc-hFBXO22b Δ20–67 mutant still coimmunoprecipitates with HA-SR (Fig. 1*D*, *lane 2*), indicating that the SFC complex is not required for SR/FBXO22 interaction.

SR and rat FBXO22a coimmunoprecipitate from rat brain homogenates, indicating that the proteins appear to interact *in vivo* (Fig. 1*F*). We did not detect any band corresponding to the smaller isoform FBXO22b in brain or cultured cells, likely because of very low levels of expression. Therefore, most subsequent experiments were carried out with the FBXO22a isoform, a more likely candidate to regulate SR. Indeed, *in situ* hybridization of mouse brain shows that FBXO22a is nearly ubiquitously expressed in all easily defined brain cell types and all brain regions (47) (available from the Allen Brain Atlas).

Harper and co-workers (33) reported that the $SCF^{hFBXO22a}$ complex ubiquitinates and regulates the steady-state levels of KDM4A, which demethylates histone H3 lysine 9 and 36 . We wondered whether hFBXO22a is also required for ubiquitination and degradation of SR by the ubiquitin-proteasomal system. We found that cotransfection of hFBXO22a with SR does not promote SR ubiquitination either with or without a proteasomal inhibitor (Fig. 2*A*). Levels of SR ubiquitination with FBXO22a were even somewhat lower than the control levels (Fig. 2*A*, compare *lanes 1* and *3*). Overexpression of hFBXO22a or hFBXO22b does not affect the [S^{35}]SR half-life in pulse-chase experiments (Fig. 2*B*), indicating the lack of a significant effect on SR turnover.

Conceivably, ectopically expressed FBXO22a may generate artifacts because of its competition with the endogenous FBXO22. To more definitely exclude a role of FBXO22a in SR ubiquitination, we employed siRNA-mediated FBXO22a knockdown strategy. We found no changes in SR ubiquitina-

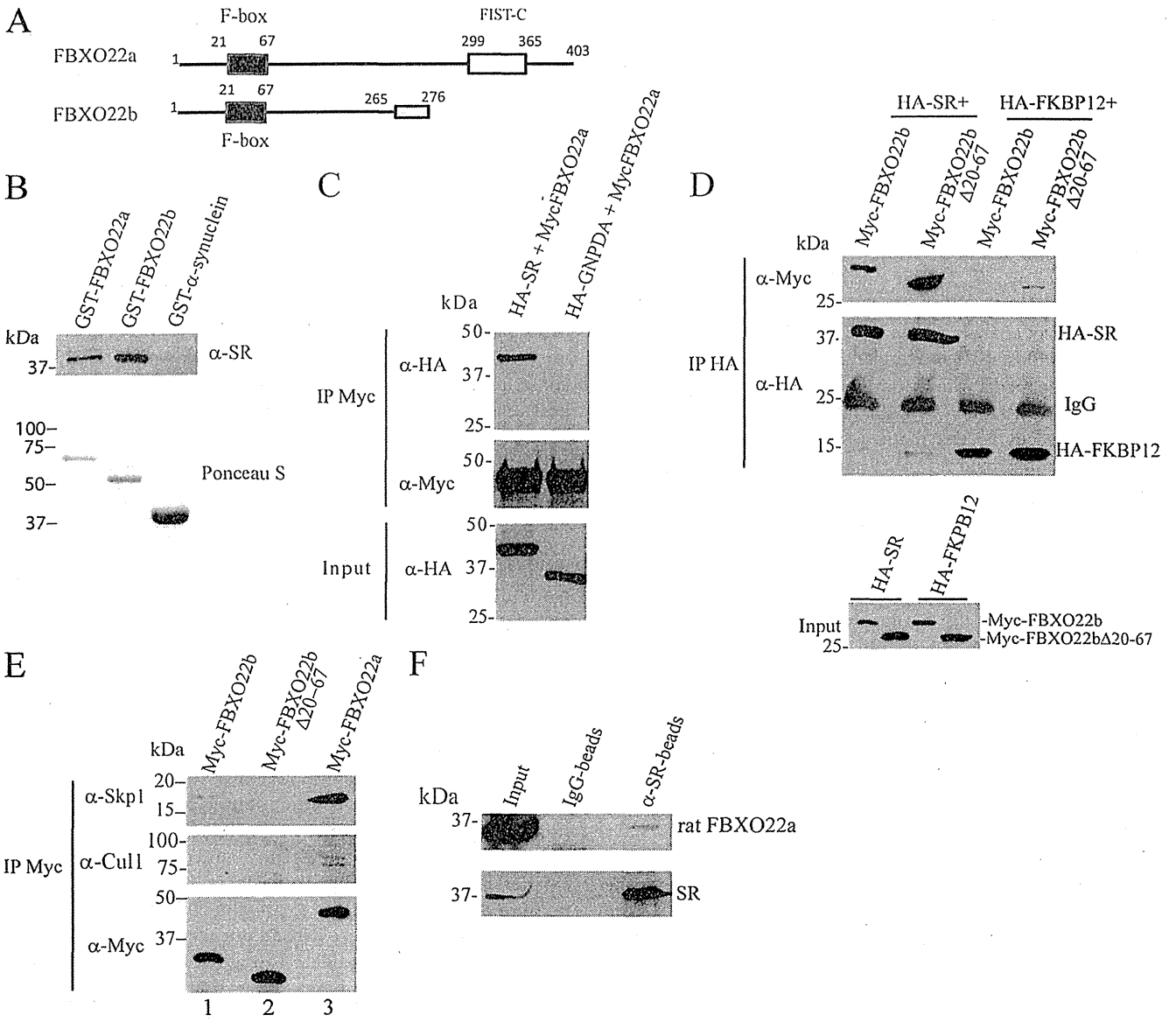

FIGURE 1. **Association of SR with FBXO22 *in vitro* and *in vivo*.** *A*, schematic of the FBXO22a and b isoforms. FBXO22b is a predicted smaller isoform that lacks the FIST C domain and whose last 11 amino acids at the C terminus are different (*gray box*). *B*, purified His-SR binds to GST-FBXO22 *in vitro*. His-SR (0.4 μg/ml) was incubated with glutathione-agarose beads containing 0.8 μg/ml GST-FBXO22a, 1.5 μg/ml GST-FBXO22b, or 30 μg/ml GST-α-synuclein. SR bound to the beads was monitored with anti-SR serum (1:1000) (*top panel*). *Bottom panel*, the GST-fusion proteins used in the binding experiments stained by Ponceau S. *C*, SR coimmunoprecipitates with FBXO22a. HEK 293 cells were cotransfected with Myc-FBXO22a and either HA-SR or HA-GNPDA (control protein), and immunoprecipitation (*IP*) was carried out with anti-Myc matrix. HA-SR or HA-GNPDA in the immunoprecipitate were detected with mouse anti-HA (1:1000) (*top panel*). Immunoprecipitated Myc-FBXO22a was detected with mouse anti-Myc (1:5000) (*center panel*). The *bottom panel* corresponds to the input (5%) probed with anti-HA. *D*, SR/FBXO22 interaction does not depend on the F-box domain. Myc-FBXO22b or Myc-FBXO22b Δ20–67 (lacking the F-box domain) coimmunoprecipitate with HA-SR but not with HA-FKBP12 control protein (*top panel*). The *center panel* corresponds to HA-SR and HA-FKBP12 immunoprecipitate probed with anti-HA. Levels of Myc-FBXO22a and Myc-FBXO22b in the input were monitored with polyclonal anti-Myc (1:1000) (*bottom panel*). The blots are representative of at least three experiments. *E*, coimmunoprecipitation of Myc-FBXO22a, Myc-FBXO22b, or Myc-FBXO22b Δ20–67 with endogenous Cul1 and Skp1 from HEK293 cells. Myc-FBXO22a interacts with both Skp1 and Cul1, which are the core components of the SCF complex. A much weaker interaction was observed with Myc-FBXO22b, whereas no binding was detectable with Myc-FBXO22b lacking the F-box region (*Δ20–67*). *Top panel*, coimmunoprecipitation with Skp1 monitored mouse anti-Skp1 (1:500). *Center panel*, coimmunoprecipitation with Cul1 monitored with mouse anti-Cul1 (1:500). *F*, SR and FBXO22A interact *in vivo*. Immunoprecipitation from rat brain homogenate with anti-SR demonstrates coimmunoprecipitation of SR to FBXO22 but not when rabbit IgG was used (*B*). The coimmunoprecipitation was checked using anti-FBXO22 (1:100, *top panel*). SR presence was verified using anti-SR serum (1:1000, *bottom panel*). The blots are representative of at least three experiments.

tion when levels of endogenous FBXO22 were decreased efficiently (Fig. 2*C*, compare *lanes 1* and *2* with *lanes 3* and *4*).

To investigate whether endogenous hFBXO22a affects SR targeting to the proteasome, we tested the effect of hFBXO22a knockdown on steady-state levels of endogenous SR in human brain glioblastoma A172 cells (Fig. 2*D*). Endogenous SR expression was unaffected by FBXO22 siRNA, which efficiently knocked down endogenous hFBXO22a expression (Fig. 2*D*). These data are consistent with the notion that hFBXO22a does not play a role in SR degradation by the ubiquitin system.

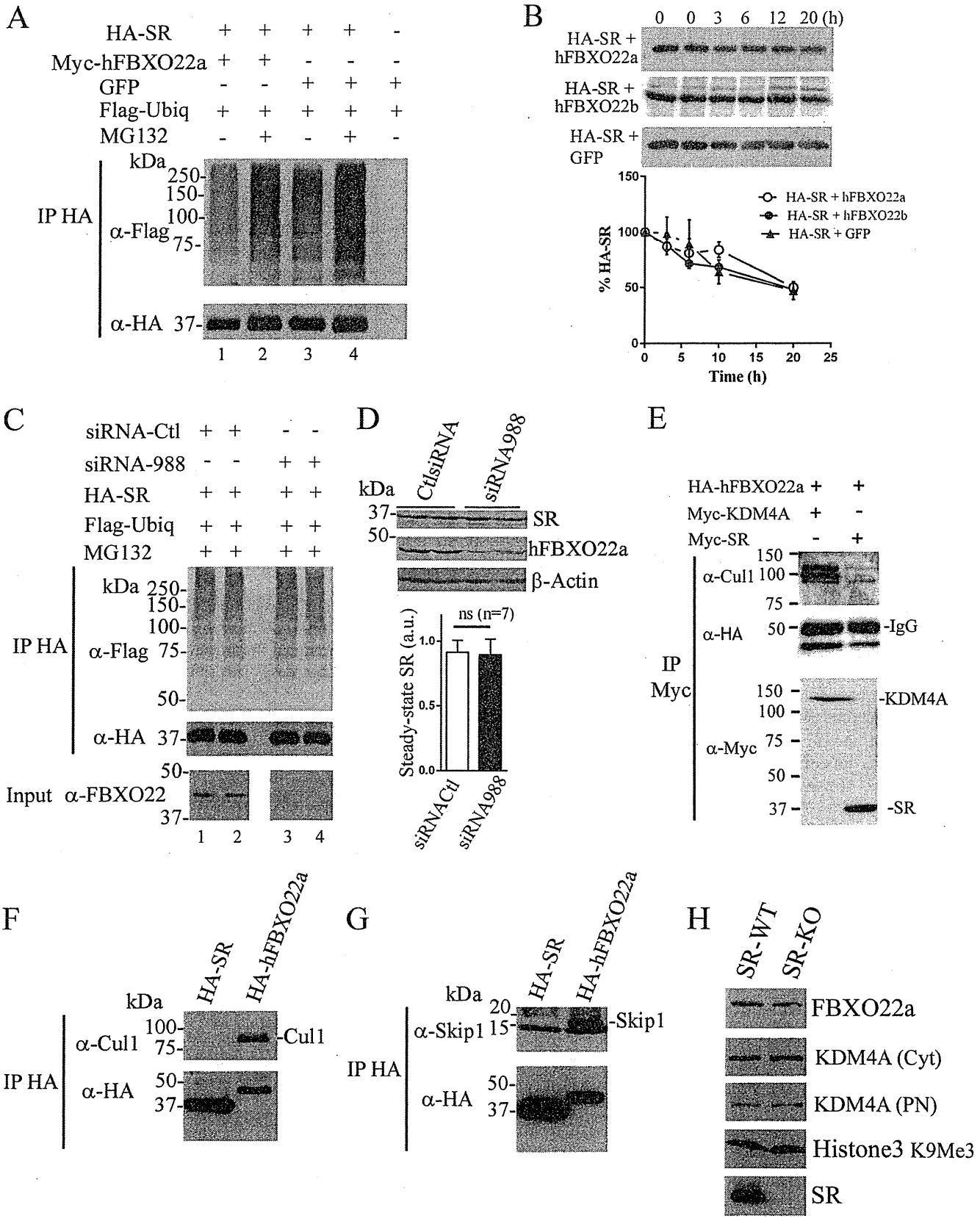

Because hFBXO22a coimmunoprecipitates with components of the SCF complex (Fig. 1*E*), we investigated whether the pool of hFBXO22a interacting with SR is associated with the SCF complex. We found that Cul1 is absent from the SR/hFBXO22 coimmunoprecipitate, indicating that SR interacts preferentially with a free hFBXO22a pool (Fig. 2*E*). As a control, we confirmed that the $SCF^{hFBXO22}$ complex substrate KDM4A coimmunoprecipitates with both hFBXO22a and Cul1 under the same experimental conditions (Fig. 2*E*) (33). Furthermore, FBXO22a, but not SR, coimmunoprecipitated with ectopically expressed Cul1 (Fig. 2*F*) or Skp1a (Fig. 2*G*). These data are consistent with the notion that SR does not interact with the $SCF^{hFBXO22}$ complex.

Does SR affect FBXO22a function? To address this question, we monitored the levels of FBXO22a and the $SCF^{FBXO22a}$ substrate KDM4A in brain homogenates from wild-type and SR-KO mice (Fig. 2*H*). We found that levels of both FBXO22a and KDM4A were unchanged in SR-KO mice, indicating that the function of $SCF^{FBXO22a}$ is not changed globally in SR-KO mice. Likewise, methylated histone 3, which is demethylated by KDM4A, was unaffected, excluding a significant effect of SR on FBXO22a targets (Fig. 2*H*).

We next examined whether FBXO22 regulates SR activity. SR binds avidly to membrane lipids, especially of the phosphoinositol type (29). This leads to inhibition of SR activity. Accordingly, NMDAR-elicited translocation of SR from the cytosol to the membrane completely inactivates D-serine synthesis in neurons (30). However, despite the apparent high affinity of SR to lipids, most of the protein is soluble in the cytosol under basal conditions. We found that FBXO22a seems to be important in keeping SR in the cytosol (Fig. 3, *A* and *B*). siRNA-mediated hFBXO22a knockdown increased severalfold the levels of endogenous SR associated to the membrane fraction of glioblastoma cells (Fig. 3*A*). Levels of endogenous SR in homogenate (Fig. 3*A*, *Hom*) were unchanged, indicating that FBXO22a does not affect SR expression. Knockdown of endogenous hFBXO22a was monitored in the homogenate (Fig. 3*A*, *Hom*). As expected, the levels of the $SCF^{FBXO22a}$ substrate KDM4A increased in the purified nucleus and membrane fraction, confirming the role of hFBXO22a in regulating KDM4A levels (33).

Similar to that seen in glioblastoma cells, infection of primary cortical neuronal cultures with shRNA to rat FBXO22a increases the levels of membrane-bound SR without changing β-tubulin levels (Fig. 3*B*). Total expression of SR was unaffected by shRNA to FBXO22a but significantly decreased the levels of endogenous FBXO22a (Fig. 3*B*, *Hom*).

Immunocytochemical experiments confirmed the biochemical findings. hFBXO22a knockdown appears to increase levels of SR that colocalizes with intracellular membranes, as seen by increased colocalization with KDEL, an endoplasmic reticulum marker (Fig. 4, *C–H*).

Because SR is inactivated upon binding to membranes (29, 30), we next examined whether the effects of hFBXO22a on SR subcellular localization may influence D-serine production. We found that siRNA-mediated knockdown of endogenous hFBXO22a in glioblastoma cells decreases endogenous D-serine production by about 40% (Fig. 4, *A* and *B*), indicating that hFBXO22a is required for optimal D-serine synthesis in the cellular environment. Similarly, lentivirus-mediated shRNA knockdown of FBXO22 in rat primary astrocytes (Fig. 4*C*) decreased D-serine production by 40% (Fig. 4*D*). Experiments employing recombinant proteins demonstrate that a 30- to 40-fold molar excess of hFBXO22a or hFBXO22b does not directly affect the activity of the soluble recombinant SR measured under standard conditions *in vitro* (Fig. 4, *E* and *F*). The data are consistent with the notion that changes in subcellular localization of SR (Fig. 3), rather than a direct effect on SR activity at the cytosol, mediate FBXO22 effect in D-serine synthesis observed in cells (Fig. 4, *A–D*).

DISCUSSION

We described a new interaction of SR with FBXO22a, which is required for optimal D-serine synthesis. We confirmed the interaction by biochemical methods and showed that knockdown of FBXO22a decreases D-serine synthesis in cells. This was associated with higher levels of SR in the membrane fraction of glioblastoma cells and primary neurons, suggesting that hFBXO22a is important for proper targeting of SR. Furthermore, changes in SR subcellular localization by FBXO22 are observed in both glia and neuronal cells, indicating that this may be a general regulatory mechanism. Except for Golga3, a protein that affects SR half-life (48), no other SR interacting protein was demonstrated to affect its function in both glial and neuronal cells.

F-Box proteins are generally thought to play a role in the ubiquitin-proteasome system (43, 44, 49, 50). The $SCF^{FBXO22a}$ ubiquitin ligase complex regulates the degradation of KDM4A

FIGURE 2. **hFBXO22a does not affect SR turnover or targeting to the proteasome.** *A*, SR ubiquitination (*Ubiq*) is not increased when cotransfected with FBXO22a. HA-SR was cotransfected with Myc-hFBXO22a or GFP and incubated with or without MG132 (a proteasome inhibitor). HA immunoprecipitate (*IP*) was probed with mouse anti-FLAG (1:500, Sigma) to reveal ubiquitin conjugates (*top panel*). Non-ubiquitinated SR was revealed with mouse anti-HA (1:1000, *bottom panel*). *B*, SR turnover is unaffected by hFBXO22 overexpression. HA-SR was cotransfected with hFBXO22a, hFBXO22b, or GFP ($n = 3$). Cells were incubated in a medium containing [^{35}S]methionine/cysteine and chased for the indicated times (*top panel*). *Bottom panel*, PhosphorImager analysis of [^{35}S]SR. *C*, endogenous FBXO22a knockdown does not affect SR ubiquitination. HEK293 cells were cotransfected with HA-SR, FLAG-ubiquitin, siRNA to hFBXO22a, or control (*Ctl*) siRNA, and ubiquitination was revealed as in Fig. 2*A* after 12 h incubation with 30 μM MG132. *Bottom panel* (*input*), successful knockdown of endogenous hFBXO22a expression revealed with mouse anti-FBXO22 (1:1000). *D*, knockdown of endogenous hFBXO22a does not affect endogenous SR steady-state levels in A172 glioblastoma cells (*top panel*). Transfection was performed with siRNA against hFBXO22a, which down-regulated hFBXO22a expression (*center panel*). *Bottom panel*, β-actin loading control. The *graph* shows the lack of change in the steady-state levels of endogenous SR from seven independent experiments. *a.u.*, arbitrary units; *ns*, not significant. *E*, SR preferentially interacts with free FBXO22a species. Myc-SR or Myc-KDM4A was cotransfected with HA-FBXO22a and immunoprecipitated with anti-Myc. Cul1 was present in the Myc-KDM4A/HA-FBXO22a coimmunoprecipitate but absent from the Myc-SR·HA-FBXO22a complex (*top panel*). HA-FBXO22a was revealed with mouse anti-HA (1:1000, *center panel*), whereas immunoprecipitated Myc-KDM4A or Myc-SR was revealed with mouse anti-Myc (1:1000, Sigma, *bottom panel*). *F* and *G*, HA-FBXO22a, but not HA-SR, interacts with ectopically expressed Cul1 (*F*) or Skp1a (*G*). *H*, FBXO22a, KDM4A, and H3K9Me3 levels are unchanged in brain homogenates of SR-KO mice. *Cyt*, brain cytosolic fraction; *PN*, brain purified nuclear fraction. The blots are representative of at least three different experiments.

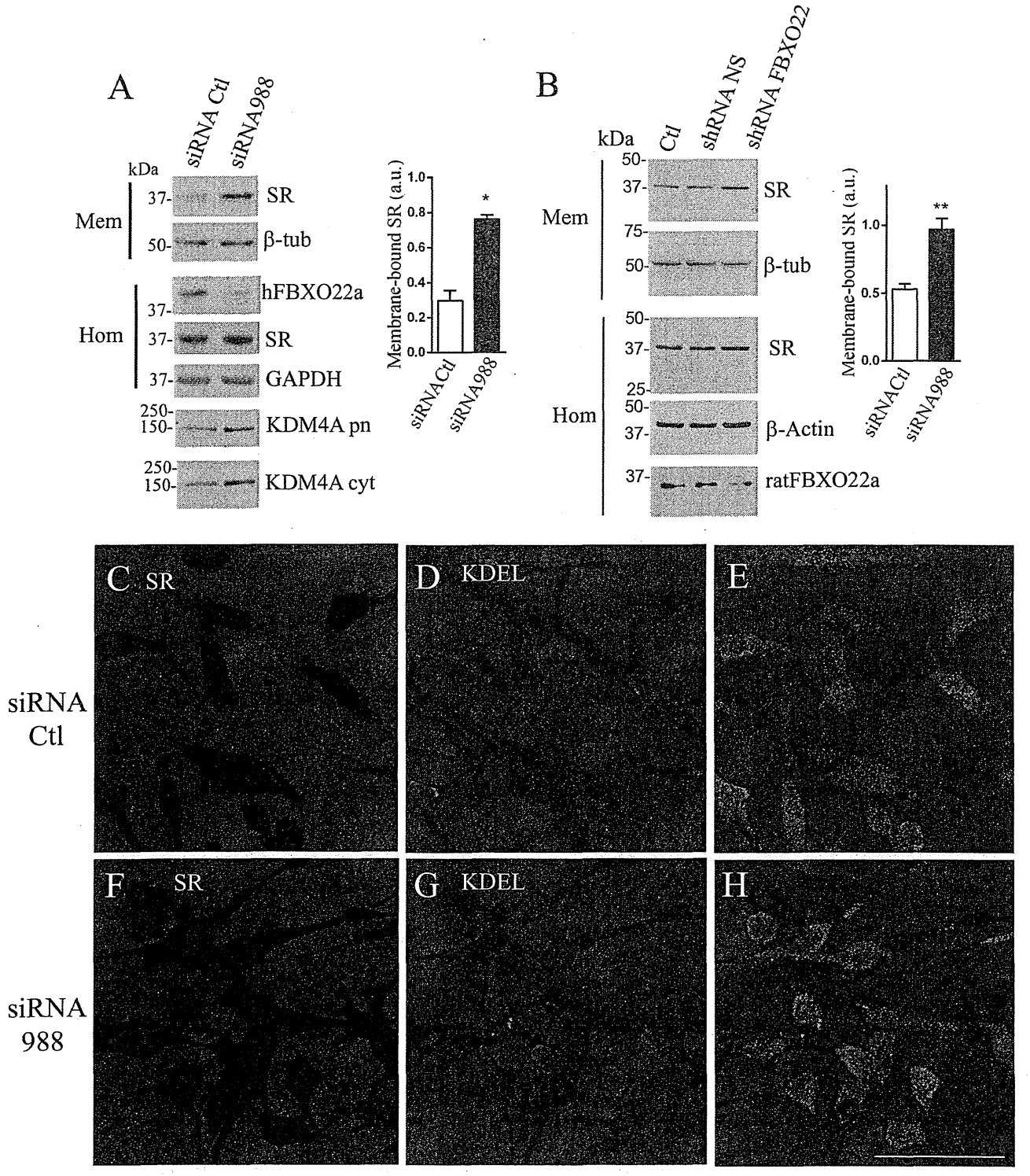

FIGURE 3. **FBXO22a primarily affects SR subcellular localization.** *A*, siRNA-mediated knockdown of endogenous hFBXO22 expression in A172 glioblastoma cells increases endogenous SR levels in the membrane fraction. Levels of endogenous SR in the membrane fraction (*Mem*) increased upon hFBXO22a knockdown, whereas β-tubulin (*β-tub*) levels were unchanged. Knockdown of endogenous hFBXO22a monitored in the homogenate fraction (*Hom*) did not affect the total expression of SR or GAPDH revealed with rabbit anti-SR (1:1000) or mouse anti-GAPDH (1:200). siRNA to hFBXO22a increased in the levels of its substrate KDM4A both in the purified nuclei fraction (*KDM4 pn*) and in the cytosolic fraction (*KDM4 cyt*), as revealed by rabbit anti-KDM4A (1:500). The *graph* depicts the increase in membrane-bound SR in three experiments. *a.u.*, arbitrary units; *Ctl*, control. *B*, knockdown of endogenous rat FBXO22 expression in primary cortical neuron cultures increases membrane-bound SR levels. Primary cortical neuron cultures were infected with a lentivirus harboring shRNA to hFBXO22 or non-silencing (*NS*) shRNA and compared with uninfected cultures (*Ctl*). Subcellular fractionation reveals an increase in the levels of endogenous membrane-bound SR with no change in the β-tubulin loading control. Total levels of SR and β-actin in homogenate (*Hom*) were unaffected, whereas shRNA to rat FBXO22 was associated with a decrease in its expression (*Hom, bottom panel*). The *graph* depicts the increase in membrane-bound SR in three experiments. *C–H*, siRNA to hFBXO22 increases the extent of colocalization of endogenous SR (*red*) with the endoplasmic reticulum marker KDEL (*green*) in A172 glioblastoma cells, as analyzed by confocal laser microscopy. Control (*C–E*) and siRNA to hFBXO22 (*F–H*) were used. *Scale bar* = 50 μm. The panels are representative of at least three different experiments. *, $p < 0.05$; **, $p < 0.01$.

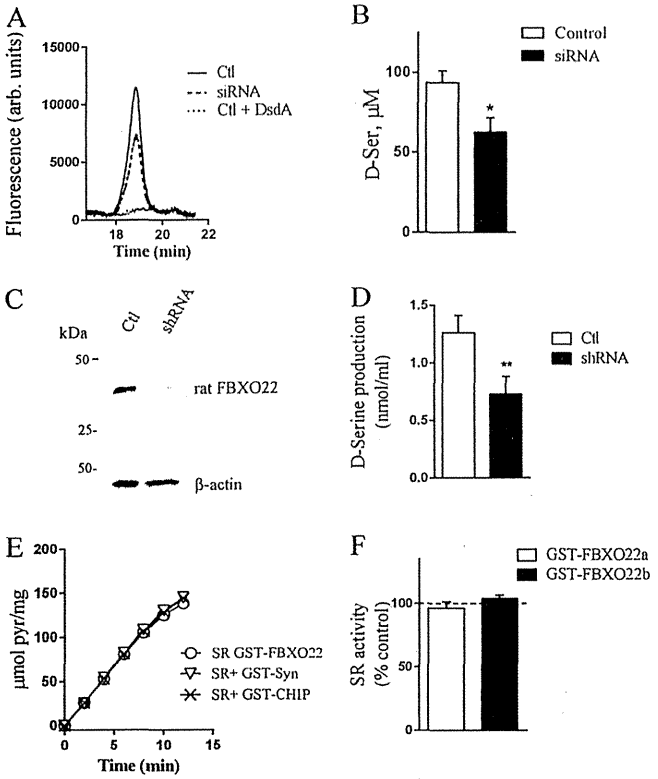

FIGURE 4. **FBXO22a is required for optimal SR activity in cells.** *A*, HPLC analysis of endogenous D-serine production in A172 glioblastoma cells revealed a discrete D-serine peak in the culture media of cells transfected with non-silencing siRNA (*Ctl*), which decreased in cells transfected with siRNA to hFBXO22. Treatment with D-serine deaminase enzyme (*DsdA*) prior to HPLC analysis abolished the peak of D-serine, indicating that it corresponds to authentic D-serine. *arb. units*, arbitrary units. *B*, quantification of D-serine (*D-Ser*) in culture media of cells transfected with non-silencing siRNA (*Ctl*) or siRNA to hFBXO22. Values represent the mean ± S.E. of four experiments with different cell cultures. *C*, knockdown of endogenous rat FBXO22 in primary astrocyte cultures infected with lentivirus containing FBXO22 shRNA when compared with non-silencing shRNA. *D*, FBXO22 knockdown decreases D-serine production in primary astrocyte cultures. *E* and *F*, lack of effect of hFBXO22a (*E* and *F*) or hFBXO22b (*F*) on SR activity *in vitro*. A 30-fold molar excess of GST-hFBXO22 isoforms did not affect His-SR activity when compared with GST-α-synuclein or GST-CHIP controls. Values represent the mean ± S.E. of at least three experiments with different protein preparations. *, $p < 0.05$.

and, ultimately, the levels of histone 3 methylation and transcription of KDM4A target genes (33). The interaction of FBXO22a with KDM4A is mediated via its FIST domain, whereas the F-Box motif is required for binding to SKP1 at the SCF complex (33). Conversely, we found that SR still interacts with an FBXO22 mutant that lacks both FIST and the F-Box motif (hFBXO22b Δ20–67), indicating that both of these domains are not required for the SR-FBXO22 interaction.

Our data indicate that FBXO22a has a non-canonical role in regulating SR activity by primarily affecting its intracellular localization. A lack of effect on SR ubiquitination with either ectopic expression of FBXO22a or siRNA knockdown indicates that SR is not a substrate of $SCF^{FBXO22a}$. Furthermore, FXBO22a does not change the SR half-life or steady-state levels. On the other hand, we found that FBXO22a is required for SR activity in cells by preventing the accumulation of membrane-bound SR species, which is inactive toward D-serine synthesis (30). This effect appears to be mediated by free FBXO22a species without the participation of the $SCF^{FBXO22a}$ complex.

A number of F-box-containing proteins play additional roles that are not related to their ubiquitination activity as components of the SCF ubiquitin-ligase complex (51–53). Emi1/Rca1 is an F-box protein that inhibits the anaphase-promoting complex/cyclosome. The anaphase-promoting complex/cyclosome is regulated by cyclin-B, whose destruction is blocked by Emi1, but does not require its F-box region (54, 55). Fbxo7 associates with Cdk6 and functions as an assembly scaffold without affecting the ubiquitination of the subunits (56). Another F-box-containing protein, Fbs1, functions as a chaperone and prevents aggregation of glycoproteins (57).

How does FBXO22a modulate SR localization and D-serine production? SR displays lipid binding motifs that mediate its binding to inositol phospholipids (29). Conceivably, FBXO22a may function as a SR chaperone and occlude its lipid-binding region. This will prevent SR interaction with membranes, known to be deleterious for SR activity (29, 30). We found that knockdown of endogenous FBXO22 led to an increase in the colocalization of SR with KDEL, suggesting the presence of SR in the endoplasmic reticulum network. Proteins departing from the endoplasmic reticulum are known to undergo different posttranslational modifications that may also contribute to SR inhibition.

FBXO22a contains a C-terminal FIST-C domain (Fig. 1*A*) involved in signal transduction and may bind small ligand molecules, possibly amino acids or their derivatives (46). Even though FBXO22-SR interaction was not mediated by the FIST domain, it is conceivable that this region provides another layer of regulation of D-serine dynamics.

In sum, our data disclose an atypical role of FBXO22 unrelated to the ubiquitin system. FBXO22 enhances SR activity primarily by preventing its binding to membranes. Small molecules that disrupt SR-FBXO22 interaction provide a new strategy to inhibit D-serine production and prevent the overactivation of NMDARs that occurs following stroke and neurodegenerative conditions.

Acknowledgments—We thank Dr. Dina Rosenberg, Goren Kolodney, and Hazem Safory for help with primary culture preparations, Dr. Elena Dumin for advice, and Edith Suss-Toby for confocal microscopy assistance.

REFERENCES

1. Traynelis, S. F., Wollmuth, L. P., McBain, C. J., Menniti, F. S., Vance, K. M., Ogden, K. K., Hansen, K. B., Yuan, H., Myers, S. J., and Dingledine, R. (2010) Glutamate receptor ion channels: structure, regulation, and function. *Pharmacol. Rev.* **62,** 405–496
2. Johnson, J. W., and Ascher, P. (1987) Glycine potentiates the NMDA response in cultured mouse brain neurons. *Nature* **325,** 529–531
3. Mothet, J. P., Parent, A. T., Wolosker, H., Brady, R. O., Jr., Linden, D. J., Ferris, C. D., Rogawski, M. A., and Snyder, S. H. (2000) D-Serine is an endogenous ligand for the glycine site of the *N*-methyl-D-aspartate receptor. *Proc. Natl. Acad. Sci. U.S.A.* **97,** 4926–4931
4. Panatier, A., Theodosis, D. T., Mothet, J. P., Touquet, B., Pollegioni, L., Poulain, D. A., and Oliet, S. H. (2006) Glia-derived D-serine controls NMDA receptor activity and synaptic memory. *Cell* **125,** 775–784
5. Rosenberg, D., Artoul, S., Segal, A. C., Kolodney, G., Radzishevsky, I.,

Dikopoltsev, E., Foltyn, V. N., Inoue, R., Mori, H., Billard, J. M., and Wolosker, H. (2013) Neuronal D-serine and glycine release via the Asc-1 transporter regulates NMDA receptor-dependent synaptic activity. *J. Neurosci.* **33,** 3533–3544

6. Henneberger, C., Papouin, T., Oliet, S. H., and Rusakov, D. A. (2010) Long-term potentiation depends on release of D-serine from astrocytes. *Nature* **463,** 232–236
7. Mothet, J. P., Rouaud, E., Sinet, P. M., Potier, B., Jouvenceau, A., Dutar, P., Videau, C., Epelbaum, J., and Billard, J. M. (2006) A critical role for the glial-derived neuromodulator D-serine in the age-related deficits of cellular mechanisms of learning and memory. *Aging Cell* **5,** 267–274
8. Kartvelishvily, E., Shleper, M., Balan, L., Dumin, E., and Wolosker, H. (2006) Neuron-derived D-serine release provides a novel means to activate *N*-methyl-D-aspartate receptors. *J. Biol. Chem.* **281,** 14151–14162
9. Shleper, M., Kartvelishvily, E., and Wolosker, H. (2005) D-serine is the dominant endogenous coagonist for NMDA receptor neurotoxicity in organotypic hippocampal slices. *J. Neurosci.* **25,** 9413–9417
10. Wolosker, H., Blackshaw, S., and Snyder, S. H. (1999) Serine racemase: a glial enzyme synthesizing D-serine to regulate glutamate-*N*-methyl-D-aspartate neurotransmission. *Proc. Natl. Acad. Sci. U.S.A.* **96,** 13409–13414
11. Wolosker, H., Sheth, K. N., Takahashi, M., Mothet, J. P., Brady, R. O., Jr., Ferris, C. D., and Snyder, S. H. (1999) Purification of serine racemase: biosynthesis of the neuromodulator D-serine. *Proc. Natl. Acad. Sci. U.S.A.* **96,** 721–725
12. De Miranda, J., Panizzutti, R., Foltyn, V. N., and Wolosker, H. (2002) Cofactors of serine racemase that physiologically stimulate the synthesis of the *N*-methyl-D-aspartate (NMDA) receptor coagonist D-serine. *Proc. Natl. Acad. Sci. U.S.A.* **99,** 14542–14547
13. Foltyn, V. N., Bendikov, I., De Miranda, J., Panizzutti, R., Dumin, E., Shleper, M., Li, P., Toney, M. D., Kartvelishvily, E., and Wolosker, H. (2005) Serine racemase modulates intracellular D-serine levels through an α,β-elimination activity. *J. Biol. Chem.* **280,** 1754–1763
14. Balu, D. T., Li, Y., Puhl, M. D., Benneyworth, M. A., Basu, A. C., Takagi, S., Bolshakov, V. Y., and Coyle, J. T. (2013) Multiple risk pathways for schizophrenia converge in serine racemase knockout mice, a mouse model of NMDA receptor hypofunction. *Proc. Natl. Acad. Sci. U.S.A.* **110,** E2400–E2409
15. Basu, A. C., Tsai, G. E., Ma, C. L., Ehmsen, J. T., Mustafa, A. K., Han, L., Jiang, Z. I., Benneyworth, M. A., Froimowitz, M. P., Lange, N., Snyder, S. H., Bergeron, R., and Coyle, J. T. (2009) Targeted disruption of serine racemase affects glutamatergic neurotransmission and behavior. *Mol. Psychiatry* **14,** 719–727
16. Labrie, V., Fukumura, R., Rastogi, A., Fick, L. J., Wang, W., Boutros, P. C., Kennedy, J. L., Semeralul, M. O., Lee, F. H., Baker, G. B., Belsham, D. D., Barger, S. W., Gondo, Y., Wong, A. H., and Roder, J. C. (2009) Serine racemase is associated with schizophrenia susceptibility in humans and in a mouse model. *Hum. Mol. Genet.* **18,** 3227–3243
17. Inoue, R., Hashimoto, K., Harai, T., and Mori, H. (2008) NMDA- and β-amyloid1–42-induced neurotoxicity is attenuated in serine racemase knock-out mice. *J. Neurosci.* **28,** 14486–14491
18. Mustafa, A. K., Ahmad, A. S., Zeynalov, E., Gazi, S. K., Sikka, G., Ehmsen, J. T., Barrow, R. K., Coyle, J. T., Snyder, S. H., and Doré, S. (2010) Serine racemase deletion protects against cerebral ischemia and excitotoxicity. *J. Neurosci.* **30,** 1413–1416
19. Mothet, J. P., Pollegioni, L., Ouanounou, G., Martineau, M., Fossier, P., and Baux, G. (2005) Glutamate receptor activation triggers a calcium-dependent and SNARE protein-dependent release of the gliotransmitter D-serine. *Proc. Natl. Acad. Sci. U.S.A.* **102,** 5606–5611
20. Balu, D. T., Takagi, S., Puhl, M. D., Benneyworth, M. A., and Coyle, J. T. (2014) D-Serine and serine racemase are localized to neurons in the adult mouse and human forebrain. *Cell Mol. Neurobiol.* **34,** 419–435
21. Benneyworth, M. A., Li, Y., Basu, A. C., Bolshakov, V. Y., and Coyle, J. T. (2012) Cell selective conditional null mutations of serine racemase demonstrate a predominate localization in cortical glutamatergic neurons. *Cell Mol. Neurobiol.* **32,** 613–624
22. Ehmsen, J. T., Ma, T. M., Sason, H., Rosenberg, D., Ogo, T., Furuya, S., Snyder, S. H., and Wolosker, H. (2013) D-Serine in glia and neurons derives from 3-phosphoglycerate dehydrogenase. *J. Neurosci.* **33,** 12464–12469
23. Miya, K., Inoue, R., Takata, Y., Abe, M., Natsume, R., Sakimura, K., Hongou, K., Miyawaki, T., and Mori, H. (2008) Serine racemase is predominantly localized in neurons in mouse brain. *J. Comp. Neurol.* **510,** 641–654
24. Rosenberg, D., Kartvelishvily, E., Shleper, M., Klinker, C. M., Bowser, M. T., and Wolosker, H. (2010) Neuronal release of D-serine: a physiological pathway controlling extracellular D-serine concentration. *FASEB J.* **24,** 2951–2961
25. Kim, P. M., Aizawa, H., Kim, P. S., Huang, A. S., Wickramasinghe, S. R., Kashani, A. H., Barrow, R. K., Huganir, R. L., Ghosh, A., and Snyder, S. H. (2005) Serine racemase: activation by glutamate neurotransmission via glutamate receptor interacting protein and mediation of neuronal migration. *Proc. Natl. Acad. Sci. U.S.A.* **102,** 2105–2110
26. Fujii, K., Maeda, K., Hikida, T., Mustafa, A. K., Balkissoon, R., Xia, J., Yamada, T., Ozeki, Y., Kawahara, R., Okawa, M., Huganir, R. L., Ujike, H., Snyder, S. H., and Sawa, A. (2006) Serine racemase binds to PICK1: potential relevance to schizophrenia. *Mol. Psychiatry* **11,** 150–157
27. Ma, T. M., Abazyan, S., Abazyan, B., Nomura, J., Yang, C., Seshadri, S., Sawa, A., Snyder, S. H., and Pletnikov, M. V. (2013) Pathogenic disruption of DISC1-serine racemase binding elicits schizophrenia-like behavior via D-serine depletion. *Mol. Psychiatry* **18,** 557–567
28. Mustafa, A. K., Kumar, M., Selvakumar, B., Ho, G. P., Ehmsen, J. T., Barrow, R. K., Amzel, L. M., and Snyder, S. H. (2007) Nitric oxide *S*-nitrosylates serine racemase, mediating feedback inhibition of D-serine formation. *Proc. Natl. Acad. Sci. U.S.A.* **104,** 2950–2955
29. Mustafa, A. K., van Rossum, D. B., Patterson, R. L., Maag, D., Ehmsen, J. T., Gazi, S. K., Chakraborty, A., Barrow, R. K., Amzel, L. M., and Snyder, S. H. (2009) Glutamatergic regulation of serine racemase via reversal of PIP2 inhibition. *Proc. Natl. Acad. Sci. U.S.A.* **106,** 2921–2926
30. Balan, L., Foltyn, V. N., Zehl, M., Dumin, E., Dikopoltsev, E., Knoh, D., Ohno, Y., Kihara, A., Jensen, O. N., Radzishevsky, I. S., and Wolosker, H. (2009) Feedback inactivation of D-serine synthesis by NMDA receptor-elicited translocation of serine racemase to the membrane. *Proc. Natl. Acad. Sci. U.S.A.* **106,** 7589–7594
31. Jin, J., Cardozo, T., Lovering, R. C., Elledge, S. J., Pagano, M., and Harper, J. W. (2004) Systematic analysis and nomenclature of mammalian F-box proteins. *Genes Dev.* **18,** 2573–2580
32. Harlow, E., and Lane, D. (1988) *Antibodies: a Laboratory Manual,* pp. 343–345, Cold Spring Harbor Laboratory, Cold Spring Harbor, NY
33. Tan, M. K., Lim, H. J., and Harper, J. W. (2011) SCF(FBXO22) regulates histone H3 lysine 9 and 36 methylation levels by targeting histone demethylase KDM4A for ubiquitin-mediated proteasomal degradation. *Mol. Cell. Biol.* **31,** 3687–3699
34. Haskin, J., Szargel, R., Shani, V., Mekies, L. N., Rott, R., Lim, G. G., Lim, K. L., Bandopadhyay, R., Wolosker, H., and Engelender, S. (2013) AF-6 is a positive modulator of the PINK1/parkin pathway and is deficient in Parkinson's disease. *Hum. Mol. Genet.* **22,** 2083–2096
35. Rott, R., Szargel, R., Haskin, J., Bandopadhyay, R., Lees, A. J., Shani, V., and Engelender, S. (2011) α-Synuclein fate is determined by USP9X-regulated monoubiquitination. *Proc. Natl. Acad. Sci. U.S.A.* **108,** 18666–18671
36. Mullen, R. J., Buck, C. R., and Smith, A. M. (1992) NeuN, a neuronal specific nuclear protein in vertebrates. *Development* **116,** 201–211
37. Hara, M. R., Agrawal, N., Kim, S. F., Cascio, M. B., Fujimuro, M., Ozeki, Y., Takahashi, M., Cheah, J. H., Tankou, S. K., Hester, L. D., Ferris, C. D., Hayward, S. D., Snyder, S. H., and Sawa, A. (2005) *S*-nitrosylated GAPDH initiates apoptotic cell death by nuclear translocation following Siah1 binding. *Nat. Cell Biol.* **7,** 665–674
38. Brewer, G. J., Torricelli, J. R., Evege, E. K., and Price, P. J. (1993) Optimized survival of hippocampal neurons in B27-supplemented Neurobasal, a new serum-free medium combination. *J. Neurosci. Res.* **35,** 567–576
39. Zufferey, R., Nagy, D., Mandel, R. J., Naldini, L., and Trono, D. (1997) Multiply attenuated lentiviral vector achieves efficient gene delivery *in vivo*. *Nat. Biotechnol.* **15,** 871–875
40. Radzishevsky, I., and Wolosker, H. (2012) An enzymatic-HPLC assay to monitor endogenous D-serine release from neuronal cultures. *Methods Mol. Biol.* **794,** 291–297
41. Ito, T., Takahashi, K., Naka, T., Hemmi, H., and Yoshimura, T. (2007) Enzymatic assay of D-serine using D-serine dehydratase from *Saccharomyces cerevisiae*. *Anal. Biochem.* **371,** 167–172

42. Panizzutti, R., De Miranda, J., Ribeiro, C. S., Engelender, S., and Wolosker, H. (2001) A new strategy to decrease *N*-methyl-D-aspartate (NMDA) receptor coactivation: inhibition of D-serine synthesis by converting serine racemase into an eliminase. *Proc. Natl. Acad. Sci. U.S.A.* **98,** 5294–5299
43. Bai, C., Sen, P., Hofmann, K., Ma, L., Goebl, M., Harper, J. W., and Elledge, S. J. (1996) SKP1 connects cell cycle regulators to the ubiquitin proteolysis machinery through a novel motif, the F-box. *Cell* **86,** 263–274
44. Cardozo, T., and Pagano, M. (2004) The SCF ubiquitin ligase: insights into a molecular machine. *Nat. Rev. Mol. Cell Biol.* **5,** 739–751
45. Pilar, A. V., Reid-Yu, S. A., Cooper, C. A., Mulder, D. T., and Coombes, B. K. (2012) GogB is an anti-inflammatory effector that limits tissue damage during *Salmonella* infection through interaction with human FBXO22 and Skp1. *PLoS Pathog.* **8,** e1002773
46. Borziak, K., and Zhulin, I. B. (2007) FIST: a sensory domain for diverse signal transduction pathways in prokaryotes and ubiquitin signaling in eukaryotes. *Bioinformatics* **23,** 2518–2521
47. Lein, E. S., Hawrylycz, M. J., Ao, N., Ayres, M., Bensinger, A., Bernard, A., Boe, A. F., Boguski, M. S., Brockway, K. S., Byrnes, E. J., Chen, L., Chen, T. M., Chin, M. C., Chong, J., Crook, B. E., Czaplinska, A., Dang, C. N., Datta, S., Dee, N. R., Desaki, A. L., Desta, T., Diep, E., Dolbeare, T. A., Donelan, M. J., Dong, H. W., Dougherty, J. G., Duncan, B. J., Ebbert, A. J., Eichele, G., Estin, L. K., Faber, C., Facer, B. A., Fields, R., Fischer, S. R., Fliss, T. P., Frensley, C., Gates, S. N., Glattfelder, K. J., Halverson, K. R., Hart, M. R., Hohmann, J. G., Howell, M. P., Jeung, D. P., Johnson, R. A., Karr, P. T., Kawal, R., Kidney, J. M., Knapik, R. H., Kuan, C. L., Lake, J. H., Laramee, A. R., Larsen, K. D., Lau, C., Lemon, T. A., Liang, A. J., Liu, Y., Luong, L. T., Michaels, J., Morgan, J. J., Morgan, R. J., Mortrud, M. T., Mosqueda, N. F., Ng, L. L., Ng, R., Orta, G. J., Overly, C. C., Pak, T. H., Parry, S. E., Pathak, S. D., Pearson, O. C., Puchalski, R. B., Riley, Z. L., Rockett, H. R., Rowland, S. A., Royall, J. J., Ruiz, M. J., Sarno, N. R., Schaffnit, K., Shapovalova, N. V., Sivisay, T., Slaughterbeck, C. R., Smith, S. C., Smith, K. A., Smith, B. I., Sodt, A. J., Stewart, N. N., Stumpf, K. R., Sunkin, S. M., Sutram, M., Tam, A., Teemer, C. D., Thaller, C., Thompson, C. L., Varnam, L. R., Visel, A., Whitlock, R. M., Wohnoutka, P. E., Wolkey, C. K., Wong, V. Y., Wood, M., Yaylaoglu, M. B., Young, R. C., Youngstrom, B. L., Yuan, X. F., Zhang, B., Zwingman, T. A., and Jones, A. R. (2007) Genome-wide atlas of gene expression in the adult mouse brain. *Nature* **445,** 168–176
48. Dumin, E., Bendikov, I., Foltyn, V. N., Misumi, Y., Ikehara, Y., Kartvelishvily, E., and Wolosker, H. (2006) Modulation of D-serine levels via ubiquitin-dependent proteasomal degradation of serine racemase. *J. Biol. Chem.* **281,** 20291–20302
49. Kipreos, E. T., and Pagano, M. (2000) The F-box protein family. *Genome Biol.* **1,** reviews s3002.1–3002
50. Ho, M. S., Ou, C., Chan, Y. R., Chien, C. T., and Pi, H. (2008) The utility F-box for protein destruction. *Cell Mol. Life Sci.* **65,** 1977–2000
51. Nelson, D. E., Randle, S. J., and Laman, H. Beyond ubiquitination: the atypical functions of Fbxo7 and other F-box proteins. *Open Biol.* 3:130131, 2013
52. Jonkers, W., and Rep, M. (2009) Lessons from fungal F-box proteins. *Eukaryot. Cell* **8,** 677–695
53. Hermand, D. (2006) F-box proteins: more than baits for the SCF? *Cell Div.* **1,** 30
54. Reimann, J. D., Freed, E., Hsu, J. Y., Kramer, E. R., Peters, J. M., and Jackson, P. K. (2001) Emi1 is a mitotic regulator that interacts with Cdc20 and inhibits the anaphase promoting complex. *Cell* **105,** 645–655
55. Zielke, N., Querings, S., Grosskortenhaus, R., Reis, T., and Sprenger, F. (2006) Molecular dissection of the APC/C inhibitor Rca1 shows a novel F-box-dependent function. *EMBO Rep.* **7,** 1266–1272
56. Laman, H., Funes, J. M., Ye, H., Henderson, S., Galinanes-Garcia, L., Hara, E., Knowles, P., McDonald, N., and Boshoff, C. (2005) Transforming activity of Fbxo7 is mediated specifically through regulation of cyclin D/cdk6. *EMBO J.* **24,** 3104–3116
57. Yoshida, Y., Murakami, A., Iwai, K., and Tanaka, K. (2007) A neural-specific F-box protein Fbs1 functions as a chaperone suppressing glycoprotein aggregation. *J. Biol. Chem.* **282,** 7137–7144

OPEN ACCESS Freely available online

PLOS | ONE

Increased Sensitivity to Inflammatory Pain Induced by Subcutaneous Formalin Injection in Serine Racemase Knock-Out Mice

Ayako Tabata-Imai, Ran Inoue, Hisashi Mori*

Department of Molecular Neuroscience, Graduate School of Medicine and Pharmaceutical Sciences, University of Toyama, Toyama, Japan

Abstract

D-Serine, an endogenous coagonist of the *N*-methyl-D-aspartate receptor (NMDAR), is widely distributed in the central nervous system and is synthesized from L-serine by serine racemase (SR). NMDAR plays an important role in pain processing including central sensitization that eventually causes hyperalgesia. To elucidate the roles of D-serine and SR in pain transmission, we evaluated the behavioral changes and spinal nociceptive processing induced by formalin using SR knock-out (KO) mice. We found that SR is mainly distributed in lamina II of the dorsal horn of the spinal cord in wild-type (WT) mice. Although the formalin injected subcutaneously induced the biphasic pain response of licking in SR-KO and WT mice, the time spent on licking was significantly longer in the SR-KO mice during the second phase of the formalin test. The number of neurons immunopositive for *c-Fos* and phosphorylated extracellular signal-regulated kinase (p-ERK), which are molecular pain markers, in laminae I-II of the ipsilateral dorsal horn was significantly larger in the SR-KO mice. Immunohistochemical staining revealed that the distribution of SR changed from being broad to being concentrated in cell bodies after the formalin injection. On the other hand, the expression level of the cytosolic SR in the ipsilateral dorsal horn significantly decreased. Oral administration of 10 mM D-serine in drinking water for one week cancelled the difference in pain behaviors between WT and SR-KO mice in phase 2 of the formalin test. These findings demonstrate that the SR-KO mice showed increased sensitivity to inflammatory pain and the WT mice showed translocation of SR and decreased SR expression levels after the formalin injection, which suggest a novel antinociceptive mechanism via SR indicating an important role of D-serine in pain transmission.

Citation: Tabata-Imai A, Inoue R, Mori H (2014) Increased Sensitivity to Inflammatory Pain Induced by Subcutaneous Formalin Injection in Serine Racemase Knock-Out Mice. PLoS ONE 9(8): e105282. doi:10.1371/journal.pone.0105282

Editor: Kazutaka Ikeda, Tokyo Metropolitan Institute of Medical Science, Japan

Received February 19, 2014; **Accepted** July 22, 2014; **Published** August 18, 2014

Funding: This work was supported by a Grant-in-Aid for Scientific Research (B) from the Ministry of Education, Culture, Sports, Science, and Technology of Japan (Grant No. 25293059; URL:http://www.mext.go.j/english/). The funders had no role in study design, data collection and analysis, decision to publish, or preparation of the manuscript.

Competing Interests: The authors have declared that no competing interests exist.

* Email: hmori@med.u-toyama.ac.jp

Introduction

D-Serine, an endogenous coagonist of the *N*-methyl-D-aspartate receptor (NMDAR), is widely distributed in the central nervous system (CNS) and is synthesized by the biosynthetic enzyme serine racemase (SR) [1,2,3]. By binding at the glycine binding site of NMDAR with an agonist, glutamate, D-serine efficiently activates NMDAR [4,5,6]. By modulating neurotransmission through NMDAR, D-serine plays important roles under physiological and pathophysiological conditions including synaptic plasticity, learning and memory, and neuronal toxicity [7,8,9,10].

Involvement of NMDAR in pain transmission has been the focus of much research in terms of central sensitization, the process for the establishment of the hyperexcitable state in the spinal cord that leads to enhanced responses to nociceptive stimuli [11]. Under repetitive noxious stimulation, excitatory postsynaptic currents (EPSCs) generated by glutamatergic transmission from nociceptors summate in postsynaptic neurons and activate NMDAR. NMDAR activation causes calcium influx, which modulates synaptic strength that leads to the enhancement of nociceptive transmission and development of hyperalgesia [12,13]. NMDAR antagonists, on the other hand, abolish or prevent the state of hyperexcitability induced by central sensitization [14]. The NMDAR antagonist ketamine has been applied as an effective analgesic adjunct for postoperative pain in humans [15].

NMDAR is basically composed of NR1 and NR2 (A - D) subunits and forms a heterotetramer between two NR1 subunits and at least one of other NR2 subunits [16]. The NR1 subunits are distributed throughout the gray matter of the spinal cord, whereas the NR2A subunit is concentrated in laminae III and IV and the NR2B subunit in lamina II of the dorsal horn [17,18]. The NR2B subunit in lamina II, where nociceptive fibers terminate, is involved in neuronal plasticity and pain transmission [19,20,21]. The antagonists selective to the NR2B subunits administered intrathecally attenuate the pain response in inflammatory and neuropathic pain models [22,23]. Because the distribution of D-serine in the brain closely matches that of NMDAR, particularly that containing the NR2B subunit [1,24], it has been postulated that D-serine is involved in pain transmission.

The lines of evidence of the contribution of D-serine in pain transmission are, however, controversial. In the studies using transgenic mice lacking D-amino acid oxidase (DAO), an enzyme that catalyzes the oxidative deamination of D-amino acids, Wake et al. reported that pain-related responses in the formalin test were

augmented [25], whereas Zhao et al. reported that they were attenuated [26]. DAO inhibitors administered intrathecally attenuated and reversed formalin-induced pain-related responses [27]. D-Serine directly applied to the rat dorsal horn increased NMDAR-mediated EPSCs [28]. Intrathecal administration of D-serine facilitated the tail flick reflex in response to thermal stimuli [29], and antagonized the antinociceptive effect of gabapentin [30] and lidocaine [31], or did not affect formalin-induced pain behavior [32].

In this study, we evaluated the behavioral changes and the spinal nociceptive processing in response to the inflammatory pain induced by formalin using SR knock-out (KO) mice as the control to elucidate the role of endogenous D-serine in pain transmission.

Materials and Methods

Ethics statement

The animal care and experimental protocol were approved by the Animal Experiment Committee of the University of Toyama (Approval number: A2011 MED-7) and were carried out in accordance with the Guidelines for the Care and Use of Laboratory Animals of the University of Toyama. Tissue sampling was performed under overdosing with sodium pentobarbital or halothane, and all efforts were made to minimize suffering.

Animals

Generation and genotyping of SR-KO and wild-type (WT) control mice with the pure C57BL/6 genetic background have been reported [33]. Adult (3–5 months) age-matched SR-KO and WT male mice were used in this study. Because diurnal circadian rhythm [34], ambient temperature [35], and acute stress [36,37] affect the pain threshold, the entire experiment was performed from 10:00 a.m. to 4:00 p.m. at room temperature (RT) between 21.5 and 24.5°C, after acclimatizing the mice to the experimental environment. The experiment was also performed with chemical restrain using the anesthetic halothane before formalin injection.

Antibodies and reagents

The primary antibodies and staining reagents used in immunohistochemical analysis were as follows: 1) the mouse monoclonal anti-SR antibody (BD Biosciences; 1:100), 2) the mouse monoclonal anti-NeuN antibody [Chemicon (Millipore); 1:100], 3) the rabbit anti-c-Fos antibody (Santa Cruz Biotechnology; 1:5,000), 4) the rabbit anti-p-ERK antibody (Cell Signaling Technology; 1:500), and 5) the rabbit anti-microtubule-associated protein 2 (anti-MAP2) antibody (Millipore; 1:100). The secondary antibodies used were Alexa-488- and Alexa-594-labeled species-specific antibodies (Invitrogen; 1:500). All the primary and secondary antibodies were diluted with 1% bovine serum albumin (BSA) in phosphate-buffered saline (PBS). FITC-conjugated isolectin IB4 (Vector Laboratories; 1:50 in PBS) was used for staining lamina II of the dorsal horn. For blocking nonspecific signals in the prepared tissue sections, 10% donkey normal serum in PBS was used. For p-ERK staining, 0.3% Triton-X 100 was added to the blocking and antibody-diluting solutions.

The primary antibodies used in western blot analysis were 1) the rabbit anti-SR antibody (1:500) [38], 2) the rabbit anti-actin antibody (Santa Cruz Biotechnology; 1:5,000), and 3) the rabbit anti-transferrin receptor (anti-TfR) antibody (Millipore; 1:1,000). Horseradish peroxidase (HRP)-conjugated anti-rabbit IgG (Bio-Rad; 1:10,000) was used as the secondary antibody.

Immunohistochemical analysis

Mice were deeply anesthetized with sodium pentobarbital (100 mg/kg body weight, IP) and transcardially perfused with ice-cold PBS followed by 4% paraformaldehyde in PBS. The mice used in the formalin injection study were euthanized with halothane (4%) after the experiment. Their spinal cords were harvested without perfusion fixation to avoid the possible loss of immunohistochemical signals and postfixed in 4% paraformaldehyde in PBS at 4°C overnight. After cryoprotection with 30% sucrose in 0.1 M phosphate buffer, the lumbar enlargements of the spinal cords were cut and embedded in O.T.C. mounting medium (Tissue-Tek, Sakura Finetek Japan Co., Ltd., Tokyo). The spinal cords were transversally cut into 20-μm-thick sections with a cryostat (LEICA CM1850, Leica Instruments GmbH, Germany) and the sections from L4–L5 were morphologically identified under a light microscope.

Sections for staining with mouse monoclonal antibodies were pretreated with a mouse Ig blocking reagent (Vector Burlingame, CA). Sections for staining with an anti-p-ERK antibody were pretreated by permeabilization with ice-cold methanol and incubation at −20°C for 10 min. After 1 h incubation at RT with the blocking solution, tissue sections were incubated with primary antibodies described above at 4°C overnight. Sections were incubated with secondary antibodies for 1 h at RT. To identify lamina II of the dorsal horn, the sections were incubated with FITC-conjugated IB4 at RT for 1 h. All the sections were counterstained with 4′, 6-diamidino-2-phenylindole (DAPI) for cell nuclear visualization and coverslipped. Images were taken using a confocal laser scanning microscope, Leica TCS-SP5 (Leica Microsystems, Mannheim, Germany).

Formalin test

Nine WT and eleven SR-KO mice were used for the formalin test. The animals were individually handled for a week before the experiment to acclimatize them to the experimental environment. The formalin test was performed in accordance with the method described by Malmberg and Yaksh [39]. The mice were lightly anesthetized with halothane and 20 μl of 5% formalin solution (formaldehyde solution, Sigma-Aldrich; concentration was adjusted using sterile saline) was injected subcutaneously into the dorsal surface of the left hind paw using a 30-gauge needle. The mice were individually placed in a mirror-backed Plexiglass chamber ($25 \times 25 \times 20$ cm^3) for observation. After a brief recovery period (less than 2 min), the mice showed normal motor function, and then pain and other spontaneous nonpain behaviors were observed and video-recorded for 120 min. The durations of pain and nonpain behaviors were analyzed over periods of 1–5 min and 6–10 min, and at 10 min intervals after that until 120 min. The mice were euthanized with halothane (4%) 30 min after the formalin test, and their spinal cords were sampled for further analysis.

For the formalin test after oral administration of D-serine, nine WT and ten SR-KO mice were used. D-Serine (Wako, Japan) was dissolved in water at 10 mM and was administered to the WT and SR-KO mice with drinking water for one week. The formalin test and pain behavioral analysis were performed as described above.

Behavioral analysis

Mouse behaviors observed during the formalin test were analyzed using the recorded video images. Licking of the formalin-injected paw was considered as a pain behavior [40] and the time spent on licking was visually determined in units of seconds. Other spontaneous behaviors, such as walking (moving forward or backward on four limbs), rearing (standing on hind legs

with the stifle extended), grooming, and crouching, were considered to be nonpain behaviors and the duration was determined in units of seconds. Behaviors were analyzed by an experimenter who was blind to the genotype of the mice used in the study.

Counting of c-Fos- and p-ERK-immunopositive neurons in dorsal horn of mice after formalin test

The spinal cords harvested 30 min after the formalin test were processed for immunohistochemical analysis using the following primary antibodies: mouse monoclonal anti-NeuN, rabbit polyclonal anti-cFos, and rabbit polyclonal anti-p-ERK antibodies. Neurons were identified by staining with the anti-NeuN antibody. All the sections were counterstained with DAPI for cell nuclear visualization.

Five SR-KO and five WT mice were used in this study. Four nonadjacent sections from the L4–L5 lumbar spinal cord from each mouse were randomly selected before the examination of c-Fos and p-ERK immunostaining. The images of c-Fos and p-ERK staining in the dorsal horn ipsilateral to the formalin-injected hind paw were evaluated. When c-Fos or p-ERK staining in a cell was colocalized with nuclear staining (DAPI), the cell was counted as c-Fos- or p-ERK-positive. The numbers of c-Fos-positive cells within the IB4-stained area and p-ERK-positive cells in laminae I-II were manually counted.

Western blot analysis of membrane and cytosolic fraction samples from dorsal horn of lumbar spinal cord ipsilateral to formalin-injected hind paw of WT mice

Nine WT mice were used in this study. The mice were lightly anesthetized with halothane, and 20 μl of 5% formalin solution was injected into the left hind paw as in the formalin test described above. The mice were grouped into three, and their spinal cords were sampled 0 min, 30 min, and 90 min after the injection. The dorsal horn of the lumbar spinal cord ipsilateral to the injection site was processed using the method described by Huttner et al. [41] and Balan et al. [42] with slight modifications as follow. A sample of the dorsal horn ipsilateral to the injection site from each mouse was homogenized in HEPES-buffered sucrose [320 mM sucrose, 4 mM HEPES/NaOH (pH 7.3)] supplemented with protease inhibitors (Protease Inhibitor Cocktail, Nacalai Tesque, Kyoto, Japan) using a homogenizer. The homogenate was centrifuged at 1,200 x *g* for 15 min at 4°C to remove cell nuclei and debris. The supernatant was centrifuged at 200,000 x *g* for 120 min at 4°C to obtain cytosolic and membrane fractions. Protein extracts of 11–20 μg (the same weight for each electrophoresis run) were fractionated by SDS-PAGE and fractionated proteins were transferred onto a polyvinylidine difluoride (PVDF) membrane. After blocking with 5% skim milk in PBS containing 0.1% Tween-20, the PVDF membrane was incubated with rabbit anti-SR, rabbit anti-actin, and rabbit anti-TfR antibodies at 4°C overnight. Following the incubation with the appropriate secondary antibody for 40 min at RT, protein bands were detected using an ELC chemiluminescence detection system (Image Quant LAS 400 mini, GE Healthcare, Sweden). The detected protein bands were quantified using Image Quant TL software (GE Healthcare, Sweden).

Measurement of SR fluorescence intensity in somata of neurons in dorsal horn after formalin injection in WT mice

Six WT mice were used in this study. The mice were lightly anesthetized with halothane, and 20 μl of 5% formalin solution was injected into the left hind paw as in the formalin test described above. The mice were grouped into three and their spinal cords were sampled 0 min, 30 min, and 90 min after the injection. The L4–L5 spinal cords were processed for double immunohistochemical analysis using mouse monoclonal anti-SR and rabbit polyclonal anti-MAP2 antibodies as the primary antibodies. All the sections were counterstained with DAPI for cell nuclear visualization. The immunopositivity for SR and MAP2 in the dorsal horn ipsilateral to the injection site was evaluated. In the set of images obtained from 0 min and 90 min after formalin injection, ten cells that showed the colocalized signals of SR and MAP2 were selected for further analysis. The regions of interest (ROIs) were set as an ellipse (the longest diameter; 7.9±0.3 μm) around the selected cells and the fluorescence intensities of SR and MAP2 within the ROI were measured using the publicly available Java image-processing program ImageJ (National Institute of Health, Bethesda, MD).

Statistical analyses

All numerical data are presented as means ± S.E.M. The data of the formalin test were examined by two-way repeated measures analysis of variance (RM ANOVA followed by the Tukey-Kramer post-hoc test as indicated. Differences in the numbers of c-Fos- and p-ERK-positive cells in the dorsal horn between the SR-KO and WT mice, and the fluorescence intensity of SR 0 min and 90 min after formalin injection were compared by the unpaired Student's t-test. The SR protein expression levels in the cytosolic and membrane fractions 0 min, 30 min, and 90 min after formalin injection were compared by one-way ANOVA followed by the Tukey-Kramer post-hoc test as indicated. In all comparisons, values of $p<0.05$ were considered significant.

Results

Serine racemase in the spinal cord was distributed mainly in lamina II of the dorsal horn

In the central nervous system, SR is predominantly distributed in neurons of the cerebral cortex, olfactory bulb, olfactory tubercle, hippocampus, and striatum, and is weakly expressed in the cerebellum and brain stem [33]. We first examined the distribution pattern of SR in the spinal cord using SR-KO mice as the negative control. Immunofluorescence staining of SR revealed that SR was distributed mainly in the superficial part of the dorsal horn and was weakly expressed in the cell bodies in the ventral horn (Fig. 1-A). At a higher magnification, SR signals were also found to colocalize with DAPI nuclear staining (Fig. S1). In contrast, no SR signals were detected in the spinal cord of SR-KO mice (Fig. 1-B), suggesting the specificity of SR immunostaining in our study. To determine the localization of SR in the dorsal horn in the Rexed laminae, we performed double fluorescence staining of SR and IB4, which binds nonpeptidergic afferents and terminates on the middle one-third of lamina II [43,44]. The double fluorescence staining demonstrated that SR in large amounts is distributed in laminae I - III and is concentrated in lamina II of the dorsal horn (Fig. 1-C-E).

SR-KO mice showed increased pain sensitivity in the second phase of the formalin test

As a potent coagonist of NMDAR, SR in lamina II indicates that D-serine has a role in pain transmission, especially in relation to inflammation. To elucidate the involvement of SR in nociceptive transduction, we conducted the formalin test, a model for inflammatory pain [40], using SR-KO and WT mice.

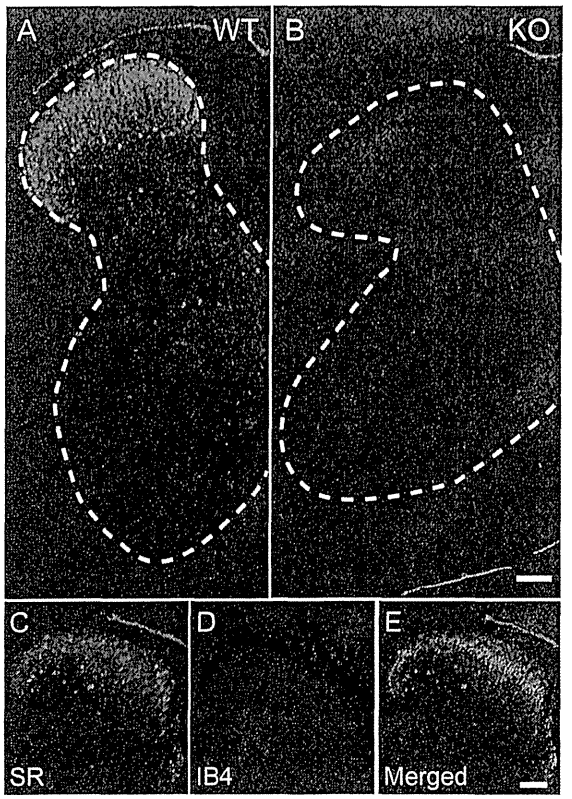

Figure 1. Distribution of immunofluorescence staining of serine racemase (SR) in lumbar spinal cord. (A) SR (green) is mainly distributed in the superficial part of the dorsal horn of the WT mice. (B) No SR signals (green) are detected in the spinal cord of the SR-KO mice. The dorsal part is the upper side. The bar indicates 100 μm in A and B. (C-E) The double immunofluorescence staining of SR (green) and IB4 (magenta), a marker of lamina II of the dorsal horn, indicates that SR is predominantly distributed in lamina II. The bar indicates 75 μm in C-E. The dotted lines in A and B are the outline of the gray matter of the spinal cord.
doi:10.1371/journal.pone.0105282.g001

Formalin subcutaneously injected into the hind paw induces a biphasic nociceptive response: immediate and intense responses with a transient quiescent period (phase 1: 1–10 min) followed by a prolonged tonic response (phase 2: 11–120 min) [39,45]. Phase 1 of the pain behavior (i.e., paw licking) is caused by the direct effect of formalin on nociceptors, which evokes intense but short-duration pain behavior, and phase 2 of the behavior is induced by inflammatory responses caused by formalin [39,46,47] and is prevented by NMDA antagonists [14]. Following the formalin injection, both WT and SR-KO mice demonstrated typical biphasic responses. The duration of the pain behavior, that is, licking on the formalin-injected paw, in phase 2 significantly increased in SR-KO mice (two-way RM ANOVA), WT vs SR-KO, $F = 8.907$, $p < 0.01$). There were no significant differences in the intensity of the pain behavior between the SR-KO and WT mice in phase 1. The licking duration in the SR-KO mice was significantly longer than that in the WT mice at 40, 100, and 110 min (Tukey-Kramer post-hoc test, $p < 0.05$), (Fig. 2-A).

In the formalin test, we investigated other behaviors that were not signs of pain: walking, rearing, grooming, and crouching. There were significant differences between the WT and SR-KO

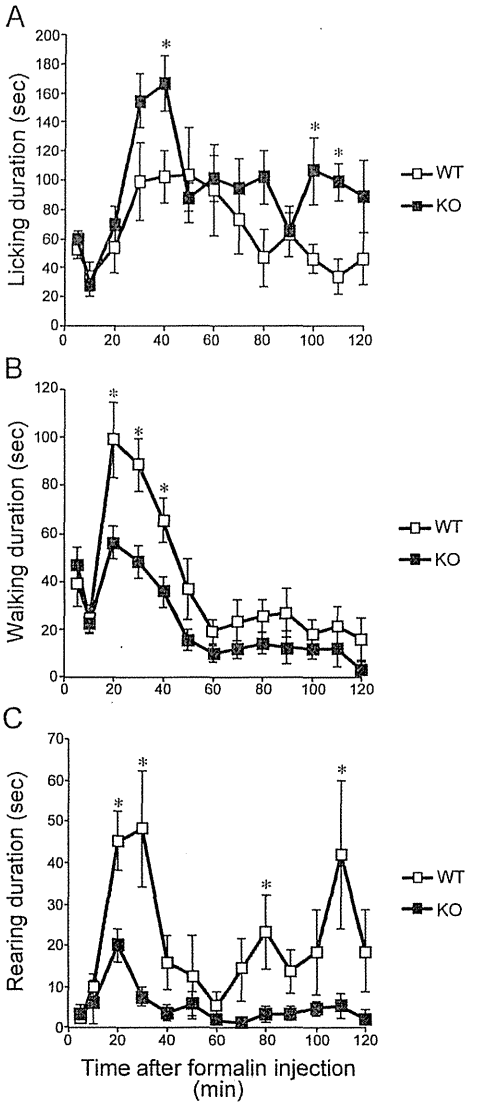

Figure 2. SR-KO mice show significantly enhanced pain behavior during the formalin test. Data from the SR-KO (n = 11, closed square) and WT (n = 9, opened square) mice are the durations of licking (A) of the formalin-injected paw (a pain behavior), and walking (B) and rearing (C) (nonpain behaviors) after formalin injection. Data are collected at 5 min intervals until 10 min after the formalin injection (0 min), then at 10 min intervals until the end of the observation period (120 min). (A) Formalin injected subcutaneously into the hind paw induced biphasic pain responses: an acute temporal but intense licking followed by a short pause (1–10 min; phase 1), and prolonged continuous tonic licking during the observation period (11–120 min; phase 2). There is no significant difference in licking duration between the SR-KO and WT mice in phase 1. However, the SR-KO mice showed significantly enhanced pain behavior in the early (40 min) and late (100 and 110 min) stages of phase 2. (B) In the early stage (20, 30, and 40 min) of phase 2, the WT mice walked significantly longer than the SR-KO mice. There is no significant difference in walking duration between the SR-KO and WT mice in phase 1. (C) The WT mice showed a significant increase in rearing duration in phase 2, especially in the early (20 and 30 min) and late (80 and 110 min) stages. There is no significant difference in rearing duration between the SR-KO and WT mice in phase 1. Values are the means ± SEM. Data were analyzed by two-way RM ANOVA followed by the Tukey-Kramer post-hoc test; * $p < 0.05$.
doi:10.1371/journal.pone.0105282.g002

mice in walking and rearing durations during phase 2 of the formalin test [two-way RM ANOVA, WT vs SR-KO, $F=8.045$, $p<0.05$ (walking), $F=9.313$, $p<0.01$ (rearing)]. The WT mice walked for a significantly longer time than the SR-KO mice at 20, 30, and 40 min of the observation period (Tukey-Kramer post-hoc test, $p<0.05$), (Fig. 2-B). The rearing durations of the WT mice were significantly longer at 20, 30, 80, and 110 min (Tukey-Kramer post-hoc test, $p<0.05$), (Fig. 2-C). There were no significant differences between the SR-KO and WT mice in grooming and crouching durations in the formalin test [two-way RM ANOVA, WT vs SR-KO, $F=0.61$, $p>0.05$ (grooming), $F=0.33$, $p>0.05$ (crouching); data not shown].

The nociceptive cells in the dorsal horn of SR-KO mice showed a markedly high activity during the formalin test

To verify the changes in neuronal activity in the dorsal horn of the spinal cord, we conducted an immunohistochemical study using the antibodies to c-Fos and phosphorylated ERK (p-ERK). c-Fos is the protein encoded by the protooncogene *c-fos* and has been extensively used as the marker of neuronal activity in pain [48,49,50]. As an immediate early gene, the transcriptional activation of *c-fos* occurs within minutes after stimulation and the expression level of the protein peaks about 2 h after the induction of gene transcription. The level of formalin-induced c-Fos expression returns to the baseline 8–24 h after formalin injection [50,51]. p-ERK has recently been commonly used as a nociceptive specific marker in many pain studies [51,52,53,54]. The p-ERK expression in response to noxious stimuli is reported to be transient: rapid onset and peaking at 2–10 min, and returning to the baseline 1–2 h after formalin injection [51,55]. The high p-ERK expression levels continue along with the pain behaviors [52]. In our formalin test, the pain behavior of WT and SR-KO mice continued to 120 min. Thus, we examined the p-ERK expression level 30 min after the behavioral test.

Figures 3-A and B show the immunofluorescence staining pattern of c-Fos in the L4–L5 spinal cord harvested 30 min after the behavioral test. After the formalin injection into the left hind paw, c-Fos protein signals were observed in the ipsilateral dorsal horn of the spinal cord in the SR-KO and WT mice. Double immunofluorescence staining of NeuN, a neuronal marker, showed the dense distribution of c-Fos-positive neurons in the superficial layers in the dorsal horn of the SR-KO and WT mice. The number of c-Fos-positive neurons in laminae I–II, identified using IB4, was significantly larger in the SR-KO mice ($n=5$, unpaired Student's t-test, two-tailed, WT vs SR-KO, $p<0.05$), (Fig. 3-C-E).

p-ERK-positive cells were also observed in the ipsilateral dorsal horn of the spinal cord in SR-KO and WT mice (Fig. 4-A, B). p-ERK was mainly distributed in lamina I–II of the dorsal horn, and the number of the p-ERK-positive neurons identified on the basis of NeuN signals was significantly larger in the SR-KO mice ($n=5$, unpaired Student's t-test, two-tailed, WT vs SR-KO, $p<0.01$), (Fig. 4-C).

Inflammatory stimuli decreased the cytosolic SR expression level in the ipsilateral dorsal horn and induced changes in SR localization in lamina II

Although D-serine is a potent coagonist of NMDAR, the mice lacking SR demonstrated increased sensitivity to inflammatory pain in our study. To clarify the role of SR, we examined the effects of noxious stimuli on SR localization and expression patterns on the basis of the lines of evidence suggesting the feedback inactivation of D-serine synthesis by NMDAR activity,

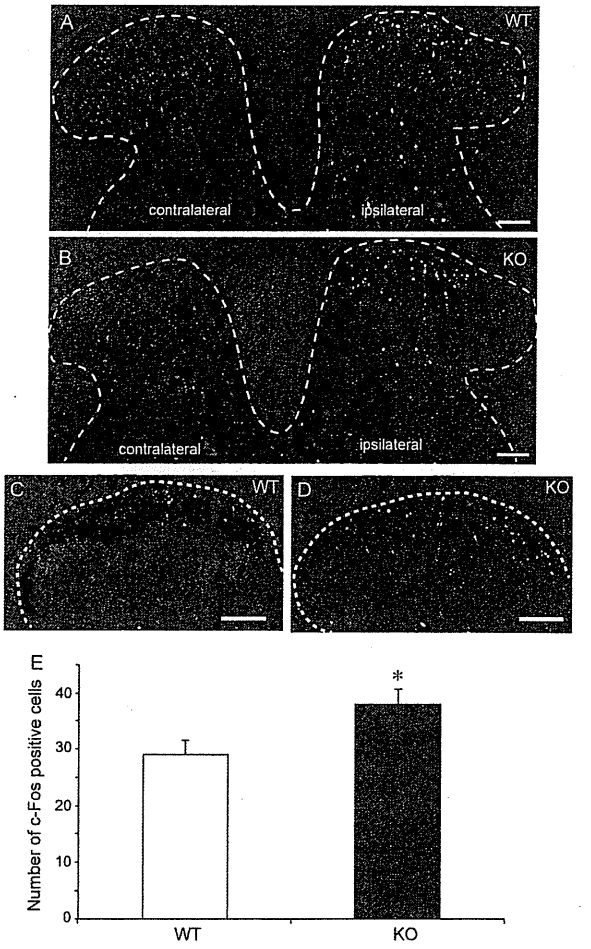

Figure 3. The number of c-Fos-positive neurons in the SR-KO mice significantly increased after the formalin test. (A, B) Immunohistochemical analysis indicates that formalin injected into the left hind paw induced c-Fos protein signals (yellow) in the ipsilateral dorsal horn neurons detected together with NeuN signals (blue) in the WT (A) and SR-KO (B) mice. The c-Fos-positive neurons are mainly distributed in the superficial layers in the dorsal horn. Bars indicate 100 μm. (C, D) Double fluorescence staining with IB4 (magenta) indicates that the c-Fos-positive (yellow) neurons are mainly distributed in laminae I-II of the dorsal horn. Bars indicate 100 μm. Dotted lines in A - D are the outline of the gray matter of the spinal cord. (E) The number of c-Fos-positive cells in laminae I-II significantly increased in SR-KO mice. Values are the means ± SEM. Data are analyzed using the unpaired t-test; * $p<0.05$ ($n=5$ for WT and SR-KO mice).
doi:10.1371/journal.pone.0105282.g003

namely, the membrane translocation of SR and the degradation of SR itself [42,56,57].

We first evaluated the SR localization in the dorsal horn of L4-L5 of the lumbar spinal cord from WT mice before and after the formalin test. Immunofluorescence signals of SR were relatively uniformly distributed in lamina II in the control mice (Fig. 5-A). A magnified image of lamina II shows densely distributed SR signals (Fig. 5-C). In contrast, immunopositivity for SR was mainly detected in the cell bodies in lamina II of the ipsilateral dorsal horn 30 min after the formalin test (Fig. 5-B). A magnified image of lamina II reveals that SR signals were concentrated in the cell bodies (Fig. 5-D). These findings suggest that the formalin

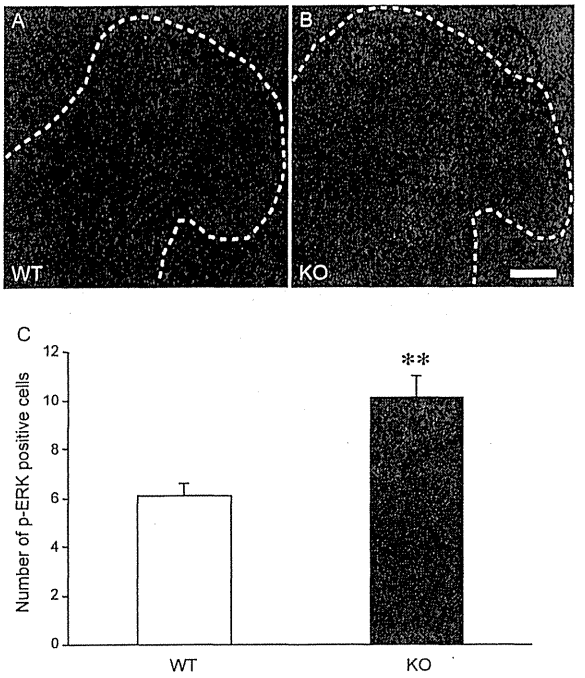

Figure 4. The number of p-ERK-positive neurons in SR-KO mice significantly increased after the formalin test. (A, B) Immunohistochemical analysis indicates that formalin injected into the left hind paw induced p-ERK signals (magenta) at the surface of the ipsilateral dorsal horn of the WT and SR-KO mice. Dotted lines in A and B are the outline of the gray matter of the spinal cord. The bar indicates 75 μm. (C) The number of p-ERK-positive neurons in laminae I–II significantly increased in the SR-KO mice. Values are the means ± SEM. Data are analyzed by the unpaired t-test; ** $p<0.01$ (n = 5 for WT and SR-KO mice).
doi:10.1371/journal.pone.0105282.g004

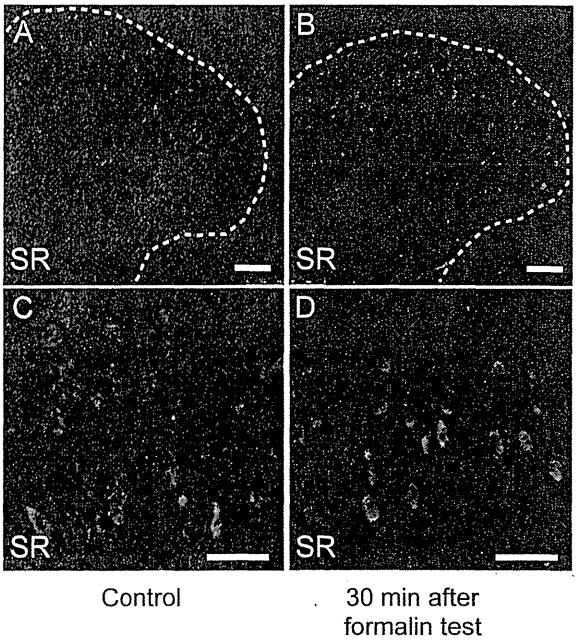

Figure 5. The distribution of SR in the dorsal horn changed after the formalin test. (A, C) Before the formalin injection, SR (green) was uniformly distributed in lamina II of the dorsal horn of the lumbar spinal cord in the WT mice. An enlarged image of lamina II demonstrates a relatively dense distribution of SR signals particularly in cell bodies. Bars indicate 50 μm. (B, D) Thirty minutes after the formalin test, the density of immunofluorescence SR signals in the ipsilateral dorsal horn decreased. A magnified image of lamina II revealed that the signals of SR concentrated in cell bodies (D). Bars indicate 50 μm. Dotted lines in A and B are the outline of the gray matter of the spinal cord.
doi:10.1371/journal.pone.0105282.g005

injection induced the changes in SR localization and expression level.

To examine the temporal changes in the level of SR expression after the formalin injection, the ipsilateral dorsal horn of the lumbar spinal cord in WT mice was harvested 0 min, 30 min, and 90 min after the formalin injection and the cytosolic and membrane fraction samples were prepared and analyzed by western blotting. After the formalin injection, the SR expression level in the cytosolic fraction significantly decreased only 90 min after the injection (one-way ANOVA, $F = 14.847$, $p<0.01$, Tukey-Kramer post-hoc test, $p<0.05$, Fig. 6-A, B). The SR expression level in the membrane fraction tended to increase after the formalin injection, but there is no significant difference in membrane SR level among the groups examined at 0, 30, and 90 min (one-way ANOVA, $F = 1.89$, $p>0.05$, Fig. 6-C, D). The expression level of the membrane SR relative to that of the total SR (cytosolic and membrane) showed no significant difference among the groups examined at 0 min, 30 min, and 90 min (one-way ANOVA, $F = 1.4235$, $p>0.05$, Fig. 6-E).

For the detailed analysis of SR localization after formalin injection, immunohistochemical analysis was carried out using the sections from the L4–L5 of the lumbar spinal cord harvested 0 min, 30 min, and 90 min after formalin injection. Immunofluorescence staining of SR indicated that the observed SR signals at lamina II of the dorsal horn at 0 min became weak 30 min after the formalin injection (Fig. 7-A1-C1, D1-F1). Double immunofluorescence staining with MAP2 (Fig. 7-A2-C2, D2-F2), the marker of neuronal somata and dendrites, revealed the colocalization of SR and MAP2 (Fig. 7-A3-C3). A magnified image of lamina II revealed that SR signals uniformly colocalized with MAP2 signals before the formalin injection, and the area of colocalization of SR and MAP2 signals decreased 30 min and 90 min after the formalin injection. Most of the merged areas were observed in the cell body after the formalin injection (Fig. 7-D3-F3). To compare the fluorescence intensity of SR in the cell body before and after the formalin injection, the fluorescence intensity of SR was normalized with MAP2 signal intensity. We found that the signal of SR in the soma 90 min after formalin injection significantly increased (n = 10, unpaired Student t-test, 0 min vs 90 min, $p<0.01$, Fig. 7-G).

Effect of exogenous D-serine on pain behavior in WT and SR-KO mice

To evaluate whether the D-serine deficit in SR-KO mice is responsible for the pain hypersensitivity, we conducted the formalin test after the administration of exogenous D-serine. Because the administration of 10 mM D-serine in drinking water for one week significantly increased the spinal D-serine level in SR-KO mice [58], we conducted the formalin test one week after oral administration of 10 mM D-serine. Formalin subcutaneously injected into the hind paw induced typical biphasic responses in WT and SR-KO mice. There were statistically no significant

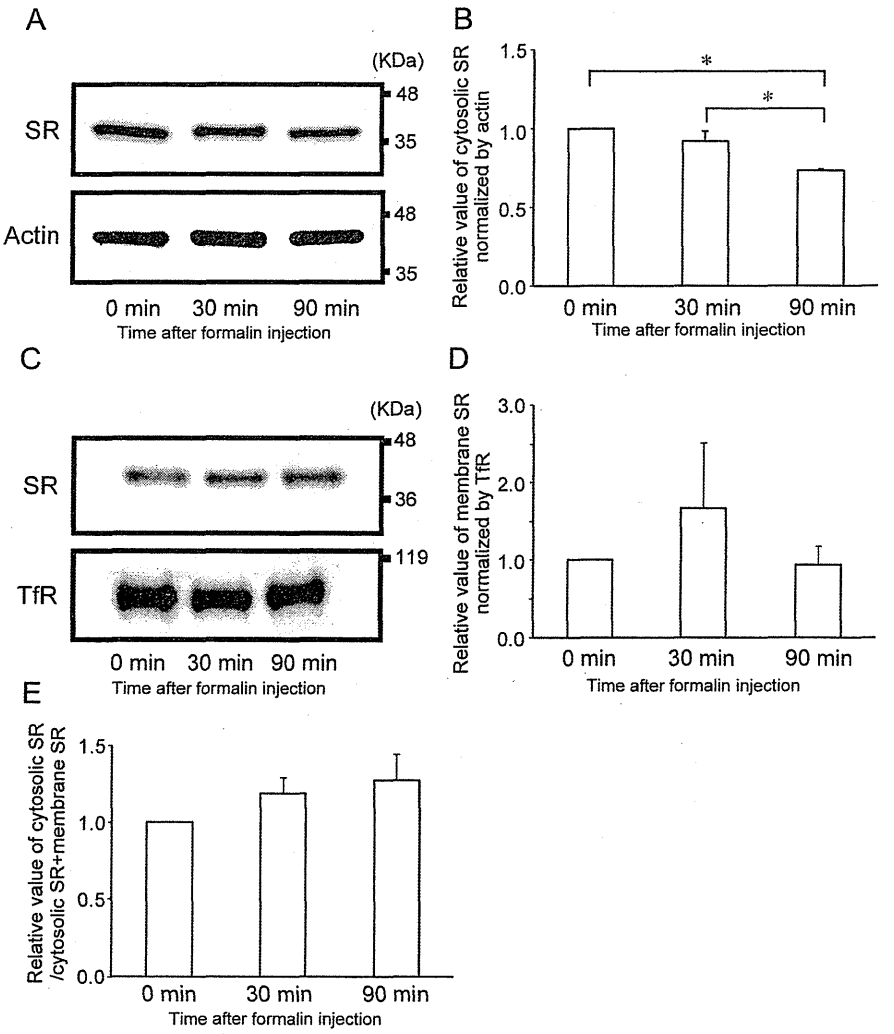

Figure 6. Cytosolic and membrane SR in the ipsilateral dorsal horn changed after the formalin test. Western blot analysis of SR in cytosolic and membrane fraction samples from ipsilateral dorsal horn of lumbar spinal cord in WT mice was performed 0 min, 30 min, and 90 min after formalin injection. (A) Western blot analysis of the cytosolic fraction revealed the decrease in SR protein expression level after formalin injection. (B) The relative SR expression level 90 min after the injection significantly decreased from the control level. The expression level of the SR protein was normalized to that of actin. (C) SR expression levels in membrane fraction before and after formalin injection. (D) Relative SR expression level after formalin injection. The expression level of the SR protein was normalized to that of the transferrin receptor protein (TfR). (E) Relative change in SR expression level in membrane fraction to those in cytosolic and membrane fractions after formalin injection. The positions of protein size markers are indicated on the right side (A, C). Values are the means ± SEM. Data are analyzed by one-way ANOVA followed by Tukey-Kramer post-hoc test; * $p<0.05$ (n = 3 for WT and SR-KO mice).
doi:10.1371/journal.pone.0105282.g006

differences in the intensity of the pain behavior between SR-KO and WT mice during the formalin test (two-way RM ANOVA, $F = 4.15$, $p = 0.06$), (Fig. 8).

Discussion

The aim of this study was to identify the role of SR in nociceptive transmission in the dorsal horn of the spinal cord using the mutant mice lacking SR. The main findings of this study were as follows: 1) SR was mainly distributed in lamina II of the dorsal horn of the spinal cord in the WT mice, 2) the SR-KO mice showed increased sensitivity to inflammatory pain induced by formalin injected subcutaneously, 3) the expression levels of the c-Fos and p-ERK proteins, the molecular markers of pain, significantly increased in laminae I-II of the ipsilateral dorsal horn neurons in SR-KO mice after the formalin test, 4) the immunopositivity level of SR decreased and the SR distribution pattern changed from being broad to being concentrated in cell bodies in lamina II after the formalin test, 5) the expression level of the SR protein significantly decreased in the cytosolic fraction 90 min after the noxious stimulation with formalin, 6) SR colocalized with MAP2, a marker of neuronal somata and dendrites, and the area of colocalization changed from being broad to being concentrated in cell bodies in lamina II after formalin stimuli, 7) D-serine administration for one week cancelled the difference in pain behaviors between WT and SR-KO mice. These findings indicate that SR in lamina II of the dorsal horn has

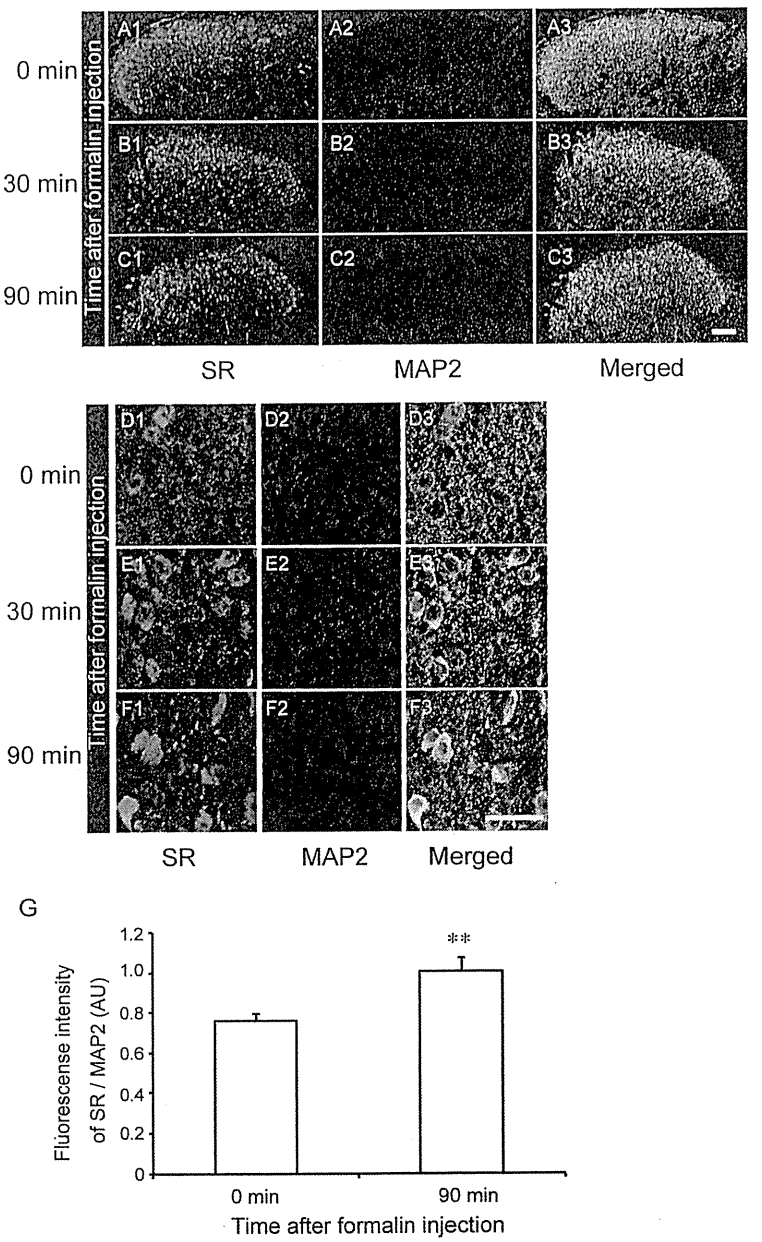

Figure 7. Immunofluorescence localization of SR in ipsilateral dorsal horn changes after formalin injection. (A-C) In WT mice, SR (green) is predominantly distributed in lamina II of the dorsal horn before formalin injection (0 min), and its signal density decreases over time after the injection (A1-C1). Double immunofluorescence staining of SR (green) and microtubule-associated protein 2 (MAP2) (red, A2-C2) indicates that SR and MAP2 colocalize in lamina II of the dorsal horn. The merged signals of SR and MAP2 are broadly distributed in the control (A3-C3). The bar indicates 75 μm in A - C. (D-F) Magnified image of areas of SR and MAP2 colocalization before and after formalin injection. Signals of SR and MAP2 are merged and densely distributed before formalin injection (D3). After formalin injection, the density of merged signals of SR and MAP2 increased in cell bodies and decreased around the cell bodies (E3, F3). The bar indicates 25 μm in D-F. (G) The relative fluorescence intensity of SR in cell bodies 90 min after the formalin injection significantly increased from the control level. The fluorescence intensity of the SR protein was normalized to that of MAP2. AU, arbitrary units. Values are the means ± SEM. Data are analyzed by the unpaired t-test; ** $p<0.01$ (n = 10 for 0 min and 90 min).
doi:10.1371/journal.pone.0105282.g007

the novel inhibitory role in pain transmission via modulation of SR localization and expression.

SR expression pattern in spinal cord

D-Serine in the brain exists at high levels in areas where NMDAR, particularly the NR2B-subunit-containing receptors, are abundant [24] and regulates NMDAR as a potent and dominant coagonist over another coagonist, glycine [5,59].

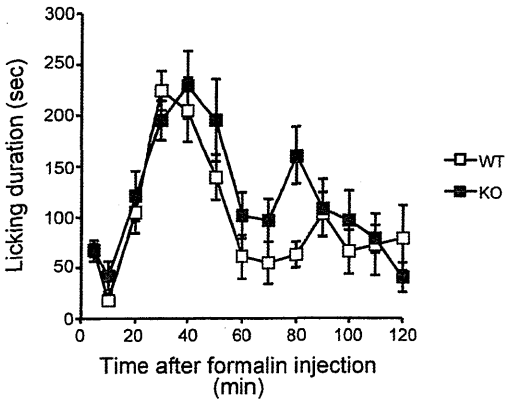

Figure 8. Effect of exogenous D-serine on pain behavior in WT and SR-KO mice. Data from the SR-KO (n = 10, closed square) and WT (n = 9, opened square) mice are the durations of licking of formalin-injected paw (a pain behavior) after formalin injection. Data are collected at 5 min intervals until 10 min after the formalin injection (0 min), then at 10 min intervals until the end of the observation period (120 min). Formalin injected subcutaneously into the hind paw induced biphasic pain responses. There is no significant difference in licking duration between the SR-KO and WT mice during the formalin test. Values are the means ± SEM. Data were analyzed by two-way RM ANOVA.
doi:10.1371/journal.pone.0105282.g008

Because the mutant mice without the SR protein show a marked decrease in the expression level of D-serine (10–20% of WT mice) in the brain [33,60,61] and because D-serine distribution closely correlates with that of SR [2,62], SR is a predominant enzyme for D-serine production [63]. Accordingly, SR has been considered an important enzyme for effective neurotransmission and synaptic plasticity via NMDAR activation. Although its expression level is low, D-serine exists in the spinal cord and is most likely produced from SR [1,58,64]. In our study, SR was found to distribute mainly in sensory neurons in lamina II of the dorsal horn. Nagy et al. immunohistochemically showed that among NMDAR subunits, the NR2B subunit is mainly distributed in lamina II of the dorsal horn [18]. This coexpression of SR and the NR2B subunit in lamina II suggests that D-serine has an important contribution to sensory transmission, particularly pain sensation, through NMDAR activation.

Formalin test

To demonstrate the involvement of SR in the pain pathway, we examined the SR-KO and WT mice by the formalin test, which induces inflammation and C-fiber-specific responses resulting in the central sensitization that requires NMDAR activation [14,39,65]. We hypothesized that if D-serine in the dorsal horn is important for central sensitization, the SR-KO mice should show attenuated pain behavior in the second phase of the formalin test. Contrary to the hypothesis, the SR-KO mice showed significantly enhanced pain behavior in the second phase. The nonpain behaviors, such as walking and rearing, were reduced in the SR-KO mice. Altogether, these findings confirm that SR-KO mice have increased sensitivity to inflammatory pain.

Hypersensitivity to inflammatory pain seen in the SR-KO mice is further supported by the increased expression levels of the c-Fos and p-ERK proteins in laminae I-II of the ipsilateral dorsal horn. Thirty minutes after the formalin test, the time when the expression level of c-Fos normally peaks and that of p-ERK continues, the numbers of c-Fos- and p-ERK-immunopositive cells were significantly larger in the SR-KO mice; therefore, the neuronal activity for nociceptive transmission is considered higher and the neuronal activation longer in the SR-KO mice.

Although it has been reported that licking behavior itself increases the c-Fos expression level [66] and decreases the p-ERK expression level [67], the effect of licking on c-Fos and p-ERK expression levels was excluded in our study because not only the expression level of c-Fos but also that of p-ERK increased in the SR-KO mice. The intense and prolonged neuronal activation in response to the formalin injection reflects the prolonged pain behavior seen in the SR-KO mice, which reinforce the idea that the SR-KO mice have increased sensitivity to inflammatory pain.

Inhibitory modulation by SR in pain pathway

Our results clearly show that SR-KO mice have increased sensitivity to inflammatory pain, indicating that the presence of SR and possibly D-serine is required for the proper inhibitory modulation in the pain pathway. There are lines of evidence showing that D-serine production is regulated by the activation and inactivation of SR. Balan et al. reported that SR translocates from the cytosol to the membrane and is inactivated by palmitoylation to inhibit D-serine synthesis after NMDAR activation [42]. Dumin et al. reported that the D-serine level is modulated via ubiquitin-dependent degradation of SR [56]. In our study, SR was found to colocalize with MAP2 and its distribution pattern changed from being broad to being concentrated in cell bodies after the formalin injection in the WT mice. On the other hand, the expression level of the SR protein significantly decreased in the cytosolic fraction. These findings indicate that the expression level of SR decreased and SR translocated into cell bodies after the formalin stimulation, suggesting that the feedback inactivation of D-serine synthesis was induced by formalin. That is, the inflammatory pain stimulation by formalin in peripheral tissues is transmitted into lamina II of the dorsal horn via C-fibers and activates NMDAR; consequently, the translocation and degradation of SR, and the decrease in cytosolic SR expression level will be induced for the inactivation of D-serine synthesis to initiate the analgesic pathway. The results of our formalin test after oral administration of D-serine for one week support this hypothesis. Miyoshi et al. reported that oral administration of D-serine significantly increases the spinal D-serine level in SR-KO mice [58]. After oral administration of D-serine, the pain behavior in phase 2 of the formalin test was enhanced in both WT and SR-KO mice to the same degree. This suggests that excess amount of D-serine in the spinal cord caused by D-serine administration cancelled the SR feedback inactivation system, which attenuates the excessive NMDAR activation.

In SR-KO mice, the SR-regulated inhibitory control is absent and glycine is the only coagonist driving NMDAR. Because D-serine activates NMDAR more efficiently than glycine does [5], it is presumable that the NMDAR barrage induced by formalin was more intense in the WT mice, at least at the beginning of the inflammatory pain transmission. Nevertheless, the SR-KO mice showed hypersensitivity to inflammatory pain. It is possible that an as yet compensatory mechanism by which the level of glycine increases in the spinal cord exists in SR-KO mice. Furthermore, Basu et al. examined the decay kinetics of NMDAR-mediated excitatory postsynaptic current recording from hippocampal cells of SR-KO mice and suggested an enhanced contribution of NR2B-containing NMDAR in the juvenile stage of SR-KO mice [60]. Hence, because the NR2B subunit is involved in pain transmission [19,20,21,22,23], an enhanced contribution of NR2B-containing NMDAR could be another possible reason for the enhanced pain transmission seen in SR-KO mice.

Our results indicate the following novel hypothetical analgesic mechanism regulated by SR. When noxious stimuli are transmitted to the dorsal horn, SR residing broadly in lamina II of the dorsal horn translocates to the cell body resulting in the inactivation of D-serine production. At the same time, the expression level of SR in the cytosol decreases, which leads to decreased D-serine production, which in turn attenuates NMDAR activation and consequently alleviates nociceptive sensation.

Conclusions

SR, which converts L-serine to the potent coagonist D-serine for NMDAR, is distributed in areas where NMDAR, especially its NR2B subunit, is abundant. Under physiological condition, D-serine plays an important role in synaptic plasticity enhancing neurotransmission. In this study, we illustrated the inhibitory modulation regulated by SR in the spinal pain pathway. This is a novel mechanism of the analgesic pathway for inflammatory pain. With the effective agents blocking D-serine production, this inhibitory pathway may provide future analgesic strategies for controlling inflammatory pain.

Supporting Information

Figure S1 Immunofluorescence localization of SR and DAPI in single optical section in dorsal horn of lumbar spinal cord. (A-C) In WT mice, SR (green) is predominantly distributed in lamina II of the dorsal horn without formalin injection (A). Double fluorescence staining of SR (green) and DAPI (blue, B) indicates that SR signals colocalize with DAPI nuclear staining (C). The bar indicates 25 μm in A - C.
(TIF)

Author Contributions

Conceived and designed the experiments: HM ATI. Performed the experiments: ATI. Analyzed the data: ATI. Contributed reagents/materials/analysis tools: RI ATI. Wrote the paper: ATI HM RI.

References

1. Hashimoto A, Nishikawa T, Oka T, Takahashi K (1993) Endogenous D-serine in rat brain: N-methyl-D-aspartate receptor-related distribution and aging. J Neurochem 60: 783–786.
2. Wolosker H, Blackshaw S, Snyder SH (1999) Serine racemase: a glial enzyme synthesizing D-serine to regulate glutamate-N-methyl-D-aspartate neurotransmission. Proc Natl Acad Sci U S A 96: 13409–13414.
3. Mothet JP, Parent AT, Wolosker H, Brady RO Jr, Linden DJ, et al. (2000) D-serine is an endogenous ligand for the glycine site of the N-methyl-D-aspartate receptor. Proc Natl Acad Sci U S A 97: 4926–4931.
4. Kleckner NW, Dingledine R (1988) Requirement for glycine in activation of NMDA-receptors expressed in Xenopus oocytes. Science 241: 835–837.
5. Matsui T, Sekiguchi M, Hashimoto A, Tomita U, Nishikawa T, et al. (1995) Functional comparison of D-serine and glycine in rodents: the effect on cloned NMDA receptors and the extracellular concentration. J Neurochem 65: 454–458.
6. Snyder SH, Kim PM (2000) D-amino acids as putative neurotransmitters: focus on D-serine. Neurochem Res 25: 553–560.
7. Yang Y, Ge W, Chen Y, Zhang Z, Shen W, et al. (2003) Contribution of astrocytes to hippocampal long-term potentiation through release of D-serine. Proc Natl Acad Sci U S A 100: 15194–15199.
8. Mothet JP, Rouaud E, Sinet PM, Potier B, Jouvenceau A, et al. (2006) A critical role for the glial-derived neuromodulator D-serine in the age-related deficits of cellular mechanisms of learning and memory. Aging cell 5: 267–274.
9. Turpin FR, Potier B, Dulong JR, Sinet PM, Alliot J, et al. (2011) Reduced serine racemase expression contributes to age-related deficits in hippocampal cognitive function. Neurobiol Aging 32: 1495–1504.
10. Inoue R, Hashimoto K, Harai T, Mori H (2008) NMDA- and beta-amyloid1-42-induced neurotoxicity is attenuated in serine racemase knock-out mice. J Neurosci 28: 14486–14491.
11. Woolf CJ (1983) Evidence for a central component of post-injury pain hypersensitivity. Nature 306: 686–688.
12. Basbaum AI, Bautista DM, Scherrer G, Julius D (2009) Cellular and molecular mechanisms of pain. Cell 139: 267–284.
13. Latremoliere A, Woolf CJ (2009) Central sensitization: a generator of pain hypersensitivity by central neural plasticity. J Pain 10: 895–926.
14. Woolf CJ, Thompson SW (1991) The induction and maintenance of central sensitization is dependent on N-methyl-D-aspartic acid receptor activation; implications for the treatment of post-injury pain hypersensitivity states. Pain 44: 293–299.
15. Laskowski K, Stirling A, McKay WP, Lim HJ (2011) A systematic review of intravenous ketamine for postoperative analgesia. Can J Anaesth 58: 911–923.
16. Mori H, Mishina M (1995) Structure and function of the NMDA receptor channel. Neuropharmacology 34: 1219–1237.
17. Watanabe M, Mishina M, Inoue Y (1994) Distinct spatiotemporal distributions of the N-methyl-D-aspartate receptor channel subunit mRNAs in the mouse cervical cord. J Comp Neurol 345: 314–319.
18. Nagy GG, Watanabe M, Fukaya M, Todd AJ (2004) Synaptic distribution of the NR1, NR2A and NR2B subunits of the N-methyl-d-aspartate receptor in the rat lumbar spinal cord revealed with an antigen-unmasking technique. Eur J Neurosci 20: 3301–3312.
19. Pedersen LM, Gjerstad J (2008) Spinal cord long-term potentiation is attenuated by the NMDA-2B receptor antagonist Ro 25-6981. Acta Physiol (Oxf) 192: 421–427.
20. Boyce S, Wyatt A, Webb JK, O'Donnell R, Mason G, et al. (1999) Selective NMDA NR2B antagonists induce antinociception without motor dysfunction: correlation with restricted localisation of NR2B subunit in dorsal horn. Neuropharmacology 38: 611–623.
21. Kovacs G, Kocsis P, Tarnawa I, Horvath C, Szombathelyi Z, et al. (2004) NR2B containing NMDA receptor dependent windup of single spinal neurons. Neuropharmacology 46: 23–30.
22. Malmberg AB, Gilbert H, McCabe RT, Basbaum AI (2003) Powerful antinociceptive effects of the cone snail venom-derived subtype-selective NMDA receptor antagonists conantokins G and T. Pain 101: 109–116.
23. Kim Y, Cho HY, Ahn YJ, Kim J, Yoon YW (2012) Effect of NMDA NR2B antagonist on neuropathic pain in two spinal cord injury models. Pain 153: 1022–1029.
24. Schell MJ, Molliver ME, Snyder SH (1995) D-serine, an endogenous synaptic modulator: localization to astrocytes and glutamate-stimulated release. Proc Natl Acad Sci U S A 92: 3948–3952.
25. Wake K, Yamazaki H, Hanzawa S, Konno R, Sakio H, et al. (2001) Exaggerated responses to chronic nociceptive stimuli and enhancement of N-methyl-D-aspartate receptor-mediated synaptic transmission in mutant mice lacking D-amino-acid oxidase. Neurosci Lett 297: 25–28.
26. Zhao W, Konno R, Zhou XJ, Yin M, Wang YX (2008) Inhibition of D-amino-Acid oxidase activity induces pain relief in mice. Cell Mol Neurobiol 28: 581–591.
27. Gong N, Gao ZY, Wang YC, Li XY, Huang JL, et al. (2011) A series of D-amino acid oxidase inhibitors specifically prevents and reverses formalin-induced tonic pain in rats. J Pharmacol Exp Ther 336: 282–293.
28. Ahmadi S, Muth-Selbach U, Lauterbach A, Lipfert P, Neuhuber WL, et al. (2003) Facilitation of spinal NMDA receptor currents by spillover of synaptically released glycine. Science 300: 2094–2097.
29. Kolhekar R, Meller ST, Gebhart GF (1994) N-methyl-D-aspartate receptor-mediated changes in thermal nociception: allosteric modulation at glycine and polyamine recognition sites. Neuroscience 63: 925–936.
30. Yoon MH, Yaksh TL (1999) The effect of intrathecal gabapentin on pain behavior and hemodynamics on the formalin test in the rat. Anesth Analg 89: 434–439.
31. Muth-Selbach U, Hermanns H, Stegmann JU, Kollosche K, Freynhagen R, et al. (2009) Antinociceptive effects of systemic lidocaine: involvement of the spinal glycinergic system. Eur J Pharmacol 613: 68–73.
32. Lu JM, Gong N, Wang YC, Wang YX (2012) D-Amino acid oxidase-mediated increase in spinal hydrogen peroxide is mainly responsible for formalin-induced tonic pain. Br J Pharmacol 165: 1941–1955.
33. Miya K, Inoue R, Takata Y, Abe M, Natsume R, et al. (2008) Serine racemase is predominantly localized in neurons in mouse brain. J Comp Neurol 510: 641–654.
34. Perissin L, Boccalon S, Scaggiante B, Petrelli L, Ortolani F, et al. (2004) Diurnal changes of tonic nociceptive responses in mice: evidence for a proalgesic role of melatonin. Pain 110: 250–258.
35. Rosland JH (1991) The formalin test in mice: the influence of ambient temperature. Pain 45: 211–216.
36. Seo YJ, Kwon MS, Shim EJ, Park SH, Choi OS, et al. (2006) Changes in pain behavior induced by formalin, substance P, glutamate and pro-inflammatory cytokines in immobilization-induced stress mouse model. Brain Res Bull 71: 279–286.
37. Cornelio AM, Mendes-Gomes J, Fugimoto JS, Morgan MM, Nunes-de-Souza RL (2011) Environmentally induced antinociception and hyperalgesia in rats and mice. Brain Res 1415: 56–62.
38. Inoue R, Yoshihisa Y, Tojo Y, Okamura C, Yoshida Y, et al. (2014) Localization of Serine Racemase and Its Role in the Skin. J Invest Dermatol 134: 1618–1626.